



# 1 Satellite-derived Constraints on the Effect of Drought Stress on 2 Biogenic Isoprene Emissions in the Southeast US

3 Yuxuan Wang<sup>1</sup>, Nan Lin<sup>1</sup>, Wei Li<sup>1</sup>, Alex Guenther<sup>2</sup>, Joey C. Y. Lam<sup>3</sup>, and Amos P. K. Tai<sup>3,4</sup>, Mark  
4 J. Potosnak<sup>5</sup>, Roger Seco<sup>6</sup>

5 <sup>1</sup>Department of Earth and Atmospheric Sciences, University of Houston, Houston, Texas, USA.

6 <sup>2</sup>Earth System Science, University of California, Irvine, Irvine, California, USA

7 <sup>3</sup>Earth System Science Programme and Graduate Division of Earth and Atmospheric Sciences, Faculty of Science,  
8 The Chinese University of Hong Kong, Hong Kong SAR, China

9 <sup>4</sup>State Key Laboratory of Agrobiotechnology and Institute of Environment, Energy and Sustainability, The Chinese  
10 University of Hong Kong, Hong Kong SAR, China

11 <sup>5</sup>Environmental Science and Studies, DePaul University, Chicago, IL, USA

12 <sup>6</sup>Institute of Environmental Assessment and Water Research (IDAEA-CSIC), Carrer Jordi Girona 18-26, 08034  
13 Barcelona, Spain

14 *Corresponding author:* Yuxuan Wang (ywang246@central.uh.edu)

15 **Abstract.** While substantial progress has been made to improve our understanding of biogenic isoprene emissions  
16 under unstressed conditions, there remain large uncertainties in isoprene emissions under stressed conditions. Here  
17 we use the US Drought Monitor (USDM) as a weekly drought severity index and tropospheric columns of  
18 formaldehyde (HCHO), the key product of isoprene oxidation, retrieved from the Ozone Monitoring Instrument (OMI)  
19 to derive top-down constraints on the response of summertime isoprene emissions to drought stress in the Southeast  
20 U.S. (SE US), a region of high isoprene emissions and prone to drought. OMI HCHO column density is found to be  
21 5.3% (mild drought) - 19.8% (severe drought) higher than that in no-drought conditions. A global chemical transport  
22 model, GEOS-Chem, with the MEGAN2.1 emission algorithm can simulate this direction of change, but the simulated  
23 increases at the corresponding drought levels are 1.4-2.0 times of OMI HCHO, suggesting the need for a drought-  
24 stress algorithm in the model. By minimizing the model-to-OMI differences in HCHO to temperature sensitivity under  
25 different drought levels, we derived a top-down drought stress factor ( $\gamma_{d\_OMI}$ ) in GEOS-Chem that parameterizes using  
26 water stress and temperature. The algorithm led to an 8.6% (mild drought) - 20.7% (severe drought) reduction in  
27 isoprene emissions in the SE US relative to the simulation without it. With  $\gamma_{d\_OMI}$  the model predicts a non-uniform  
28 trend of increase in isoprene emissions with drought severity that is consistent with OMI HCHO and a single site's  
29 isoprene flux measurements. Compared with a previous drought stress algorithm derived from the latter, the satellite-  
30 based drought stress factor performs better in capturing the regional scale drought-isoprene responses as indicated by  
31 the close-to-zero mean bias between OMI and simulated HCHO columns under different drought conditions. The  
32 drought stress algorithm also reduces the model's high bias in organic aerosols (OA) simulations by 6.60% (mild  
33 drought) to 11.71% (severe drought) over the SE US compared to the no-stress simulation. The simulated ozone  
34 response to the drought stress factor displays a spatial disparity due to the isoprene suppressing effect on oxidants,  
35 with an <1 ppb increase in O<sub>3</sub> in high-isoprene regions and a 1-3 ppbv decrease in O<sub>3</sub> in low-isoprene regions. This



36 study demonstrates the unique value of exploiting long-term satellite observations to develop empirical stress  
37 algorithms on biogenic emissions where in situ flux measurements are limited.

## 38 **1. Introduction**

39 Biogenic nonmethane volatile organic compounds (BVOCs) emitted by terrestrial ecosystems are of great importance  
40 to air quality, tropospheric chemistry, and climate due to their effects on atmospheric oxidants and aerosols (Atkinson,  
41 2000; Claeys et al., 2004; Pacifico et al., 2009). The dominant BVOC is isoprene ( $\text{CH}_2=\text{C}(\text{CH}_3)\text{CH}=\text{CH}_2$ ), comprising  
42 70% of the global total BVOC emitted from vegetation (Sindelarova et al., 2014). Isoprene emissions depend on  
43 vegetation/plant type, physiological status, leaf age, and meteorological conditions such as radiation, temperature, and  
44 soil moisture. These relationships provide the basic framework of isoprene emission models that are capable of  
45 coupling with meteorology and the land biosphere, the most widely used being the Model of Emissions of Gases and  
46 Aerosols from Nature (MEGAN) (Guenther et al., 1993, 2006, 2012, 2017). Recent work has shown stressed  
47 conditions - such as drought, heatwaves, and high winds - can induce large changes in isoprene emissions different  
48 from model predictions in the absence of those stress factors (Potosnak et al., 2014; Huang et al., 2015; Kravitz et al.,  
49 2016; Seco et al., 2015). As stressed conditions are rarely sampled by field campaigns due to their infrequent and  
50 irregular nature and hence poorly constrained, stress impacts on isoprene emissions are among the least understood  
51 aspects in our predictivity of BVOC-chemistry-climate interactions.

52 A common stress for terrestrial vegetation worldwide is drought, characterized by low precipitation, high temperature,  
53 and low soil moisture (Trenberth et al., 2014). These conditions are primary abiotic stresses that will cause  
54 physiological impacts on plants affecting photosynthesis, stomatal conductance, transpiration, and leaf area. During  
55 short-term or mild droughts, the photosynthetic rate of plants quickly decreases due to limited stomatal conductance,  
56 while isoprene is not immediately impacted because of the availability of stored carbon and because the photosynthetic  
57 electron transport is not inhibited. Isoprene can even increase by several factors due to warm leaf temperatures which  
58 increases isoprene synthase activity (Potosnak et al., 2014). During prolonged or severe drought stress, after a lag  
59 related to photosynthesis reduction, isoprene emission eventually declines because of inadequate carbon availability.  
60 This conceptualized non-monotonic response of isoprene emission to drought has been demonstrated at the Missouri  
61 Ozarks AmeriFlux (MOFLUX) field site in Missouri (Potosnak et al., 2014; Seco et al., 2015), the only available  
62 drought-relevant whole canopy isoprene flux measurements to date, and qualitatively supported by ambient isoprene  
63 concentrations monitored by regional surface networks (Wang et al., 2017). It is noteworthy that the MOFLUX data  
64 covered only two drought events (summer 2011 and summer 2012), while the surface sites are sparsely distributed  
65 with an urban focus. Thus, these observations offer only limited constraints on drought stress impacts on isoprene  
66 emissions.

67 With wide spatiotemporal coverages, satellite provides arguably the best platform to capture drought development  
68 and impacts. Satellite observations of tropospheric formaldehyde (HCHO) columns have been used as a proxy of  
69 isoprene emissions for more than a decade (Abbot et al., 2003; Palmer et al., 2003), as HCHO is formed promptly and



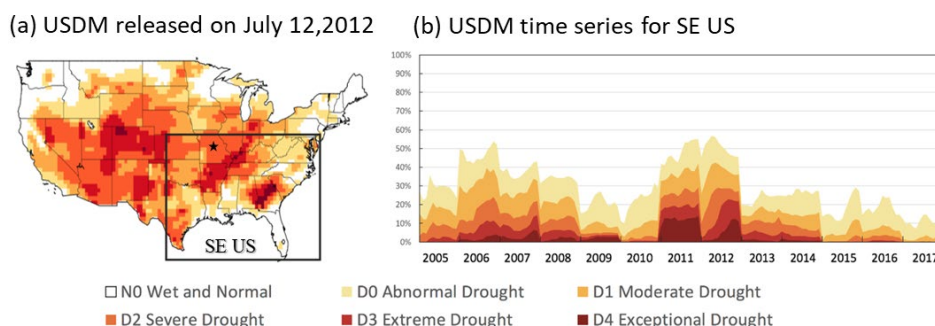
70 in high yield from isoprene oxidation (Sprengnether et al., 2002). Previous applications of satellite HCHO products  
71 provided “top-down” estimates on seasonality, magnitude, spatial distribution, and interannual variability of isoprene  
72 emissions globally and regionally (Marais et al., 2016; Kaiser et al., 2018; Stavrou et al., 2018). While most of these  
73 studies focused on *unstressed* conditions, recent efforts have shown that satellite HCHO registered drought signals on  
74 a monthly scale (Zheng et al., 2017; Naimark et al., 2021; Li et al., 2022; Opacka et al., 2022). These signals are yet  
75 to be exploited to constrain isoprene response to drought.

76 The present study aims at improving the current quantification of satellite HCHO response to drought by accounting  
77 for sub-monthly variability of drought severity. We use a weekly time scale, the finest temporal scale of drought  
78 indices available, and separate five levels of drought severity defined by the US Drought Monitor. By comparison,  
79 previous investigations used binary classification (drought or not) on the monthly time scale. Our improvement in  
80 scale is expected to better capture the nonlinear response of isoprene emissions to drought severity as described above.  
81 The study region is the Southeast United States (SE US), which has large isoprene emissions due to substantial forest  
82 coverage and is also prone to drought due to large interannual variability in precipitation (Seager et al., 2009). In  
83 addition, the MOFLUX site is located in the SE US, which will allow us to evaluate if satellite-derived drought  
84 responses of HCHO are consistent with those from isoprene flux measurements at MOFLUX. Finally, we use these  
85 HCHO signals in conjunction with models to identify the model gaps in predicting isoprene responses to drought.

## 86 **2. Data and Method**

### 87 **2.1 Drought index**

88 There are many types of drought indices focusing on different factors, including precipitation, temperature,  
89 evaporation, runoff, and the impact of drought on ecosystems and vegetation (Palmer, 1965; McKee et al., 1993;  
90 Guttman, 1999; Vicente-Serrano et al., 2010; Chang et al., 2018). Drought indices also differ by time scale. As drought  
91 by definition is a prolonged period of water deficit, the shortest time scale of drought is weekly. Here we chose the  
92 United States Drought Monitor (USDM) drought index to identify drought periods. USDM’s weekly timescale and  
93 multiple drought severity levels (Svoboda et al., 2002) provide a better delineation of drought variability than the  
94 monthly or seasonal scale used in the previous analysis of drought signals in HCHO and isoprene (Wang et al., 2017;  
95 Naimark et al., 2021).



96

97 **Figure 1. (a) Drought distribution for the second week of July 2012 based on USDM. The black star indicates the location**  
 98 **of MOFLUX site. (b) Time series of drought frequency in the study area (black box in Figure 1a) for JJA from 2005 to**  
 99 **2017. N0 (white) for wet and normal, D0 (light yellow) for abnormal drought, D1 (yellow) for moderate drought, D2 (orange)**  
 100 **for severe drought, D3 (red) for extreme drought, and D4 (brown) for exceptional drought.**

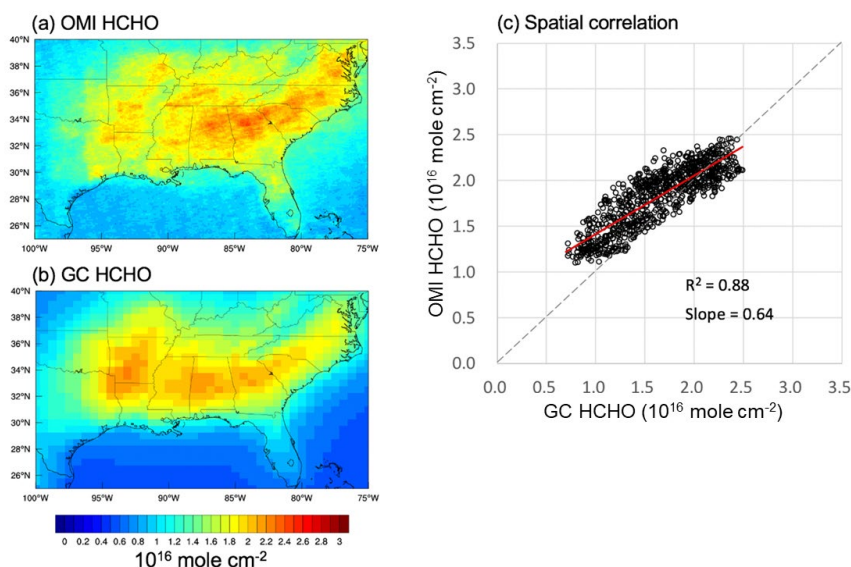
101 The USDM is a composite drought index based on six key physical indicators including the Palmer Drought Severity  
 102 Index (PDSI, Palmer, 1965), CPC Soil Moisture Model Percentiles (Huang et al., 1996), U.S. Geological Survey  
 103 (USGS) Daily Streamflow Percentiles (<http://water.usgs.gov.waterwatch/>), Percent of Normal Precipitation (Willeke  
 104 et al., 1994), Standardized Precipitation Index (SPI, McKee et al., 1993), and remotely sensed Satellite Vegetation  
 105 Health Index (Kogan, 1995). Opinions of local experts are also considered (Svoboda et al., 2002). The USDM website  
 106 (<https://droughtmonitor.unl.edu/>) provides weekly ArcGIS shapefiles of the polygons covering the whole US under  
 107 five drought levels: D0 for abnormal drought, D1 for moderate drought, D2 for severe drought, D3 for extreme drought,  
 108 and D4 for exceptional drought. We used the method of Chen et al. (2019) to rasterize and convert USDM shapefiles  
 109 to  $0.5^\circ \times 0.5^\circ$  gridded indices with -1 indicating non-drought (N0) and 0-4 for D0-D4 drought, respectively. **Figure**  
 110 **1a** displays the spatial distribution of gridded USDM indices for the second week of July 2012, which clearly depicts  
 111 the extent and severity of the infamous 2012 Great Plains drought (Hoerling et al., 2014). **Figure 1b** shows the weekly  
 112 time series of USDM indices averaged over SE US ( $75\text{--}100^\circ\text{W}$ ,  $25\text{--}40^\circ\text{N}$ , black box in Figure 1a) for the summer  
 113 months (June, July, August; JJA) of 2005 -2017, our study period. During this period, abnormal drought (D0) appeared  
 114 every summer, while extreme and exceptional drought (D3-D4) were mainly concentrated in 2006-2008 and 2010-  
 115 2012. This pattern is consistent with the long-term drought statistics from other drought indices such as SPEI and  
 116 PDSI (Svoboda et al., 2015).

## 117 2.2 OMI HCHO product

118 We used the Ozone Monitoring Instrument (OMI) v003 level 3 tropospheric formaldehyde (HCHO) column density  
 119 (OMHCHOd) as described by Chance (2019). OMI was launched on NASA's Aura satellite in 2004 and has since  
 120 provided daily global measurements of ozone ( $\text{O}_3$ ) and its precursors with a nadir spatial resolution of  $24 \times 13 \text{ km}^2$ .  
 121 Since January 2009, OMI has been suffering from a major row anomaly. OMHCHOd data processing explored all  
 122 level 2 OMHCHO observations to filter out pixels with bad formaldehyde retrievals, high cloud fractions ( $>30\%$ ),  
 123 high SZA ( $>70^\circ$ ), and pixels affected by OMI's row anomaly (Chance, 2019). The spatial resolution is  $0.1^\circ \times 0.1^\circ$ .  
 124 Zhu et al. (2016) verified the OMHCHOd data using high-precision HCHO aircraft observations obtained during



125 NASA SEAC4RS activities in SE US from August to September 2013. They showed that OMI retrievals have accurate  
 126 spatial and temporal distribution but underestimated HCHO column density. We corrected this underestimation by  
 127 applying a uniform factor of 1.59 (Zhu et al., 2016; Kaiser et al., 2018) to the OMHCHOd data. **Figure 2a** presents  
 128 the corrected OMHCHOd for the SE US averaged over JJA 2005-2017, where higher levels of HCHO are clearly seen  
 129 over forested regions in Missouri, Georgia, Arkansas, and Texas. OMHCHOd values shown hereafter are those with  
 130 the correction factor applied.



131

132 **Figure 2.** (a) Mean 2005–2017 HCHO columns for June – August over the SE US of OMI observation and (b) GEOS-Chem  
 133 simulation. (c) Scatterplot of spatial correlation between the two. The dashed line indicates the 1:1 agreement.

### 134 2.3 GEOS-Chem chemical transport model

135 We used the long-term simulation of the nested-grid GEOS-Chem global chemical transport model (version 12-02,  
 136 <http://www.geos-chem.org>) to obtain daily mean results of modeled formaldehyde columns and isoprene emissions  
 137 for North America during JJA 2005 – 2017. The simulation was driven by the Modern-Era Retrospective analysis for  
 138 Research and Applications, Version 2 (MERRA-2) meteorological data from NASA’s Global Modeling and  
 139 Assimilation Office (GMAO) with a horizontal resolution at  $0.5^\circ \times 0.625^\circ$ . Biogenic emissions were calculated using  
 140 MEGAN2.1, which is the prevailing version of MEGAN implemented in most chemical and climate models.  
 141 MEGAN2.1 has a soil dependence algorithm whose parameterization is based on plant wilting point threshold and  
 142 soil moisture (Guenther et al., 2017). However, this factor is disabled in GEOS-Chem as in many other CTMs due to  
 143 the unavailability of the required driving variables, such as wilting point and soil moisture, which cannot be simulated  
 144 well in most models (Trugman et al., 2018). Thus, outputs from the standard GEOS-Chem simulations do not have  
 145 drought effects on isoprene emissions and these outputs are referred to as NoStress\_GC. Anthropogenic emissions  
 146 over North America were from the 2011 National Emissions Inventory (NEI2011, <http://www.epa.gov/air-emissions->



147 [inventories](#)) for the United States, with historical scale factors applied to each simulating year. Open fire emissions  
148 were from GFED4 (Giglio et al., 2013) for 2005–2017.

149 To better match with OMI overpassing time, we applied a factor of 1.12 to convert daily mean HCHO concentrations  
150 archived from the model to those of 13:30 local time; this conversion factor was adopted from the summer HCHO  
151 diurnal cycle in the Northern Hemisphere mid-latitudes in Franco et al. (2016) and we assume it remains constant  
152 during the study period. Air mass factors from OMHCHOD were applied to 13:30 LT model HCHO to calculate  
153 tropospheric vertical column density at OMI overpassing time (GCHCHO\_NoStress). **Figure 2b** shows  
154 GCHCHO\_NoStress averaged over the same domain and period as OMHCHOD in **Figure 2a**. The scatter plot (**Figure**  
155 **2c**) shows a good spatial correlation between the two ( $R^2 = 0.88$ ). This correlation is consistent with other studies  
156 comparing GEOS-Chem and OMI HCHO columns in SE US during non-drought periods (Kaiser et al., 2018).

## 157 **2.4 Observations of ozone, organic aerosol, LAI, and isoprene flux**

158 To evaluate how the drought stress factor changes the simulations of surface  $O_3$  and organic aerosol (OA), we adopted  
159 the gridded ( $1^\circ \times 1^\circ$ ) hourly  $O_3$  observations created by Schnell et al. (2014) using the modified inverse distance  
160 weighting method. The dataset aggregates several networks of  $O_3$  measurements including the US Environmental  
161 Protection Agency's (EPA) Air Quality System (AQS), Clean Air Status and Trends Network (CASTNET), and  
162 Environment Canada's National Air Pollution Surveillance Program (NAPS). Following the same method, we created  
163 a gridded organic aerosol (OA) dataset using the organic carbon (OC) observations from the Interagency Monitoring  
164 of Protected Visual Environments (IMPROVE) network. A factor of 2.1 was used to convert OC to OA as suggested  
165 by other studies (Pye et al., 2017; Schroder et al., 2018). To examine the changes of leaf area index (LAI) under  
166 droughts, the MODerate resolution Imaging Spectroradiometer (MODIS) Collection 5 LAI products reprocessed by  
167 Yuan et al. (2011) with a resolution of  $0.25^\circ \times 0.25^\circ$  was used. These three datasets were further remapped through  
168 bilinear interpolation to match the spatial resolution of the USDM. The isoprene flux measurements at the MOFLUX  
169 site during 2012 May–September were used to derive a site-based drought stress algorithm. The site is located in the  
170 Ozarks regions of central Missouri ( $38.74^\circ N$ ,  $92.20^\circ W$ , black star in Figure 1a) exceeding  $\sim 10m$  above canopy. It is  
171 surrounded by a deciduous forest dominated by isoprene-emitting white and red oak species. The dataset is widely  
172 used to investigate isoprene emissions response to droughts (Potosnak et al., 2014; Seco et al., 2015; Jiang et al., 2018;  
173 Opacka et al., 2022).

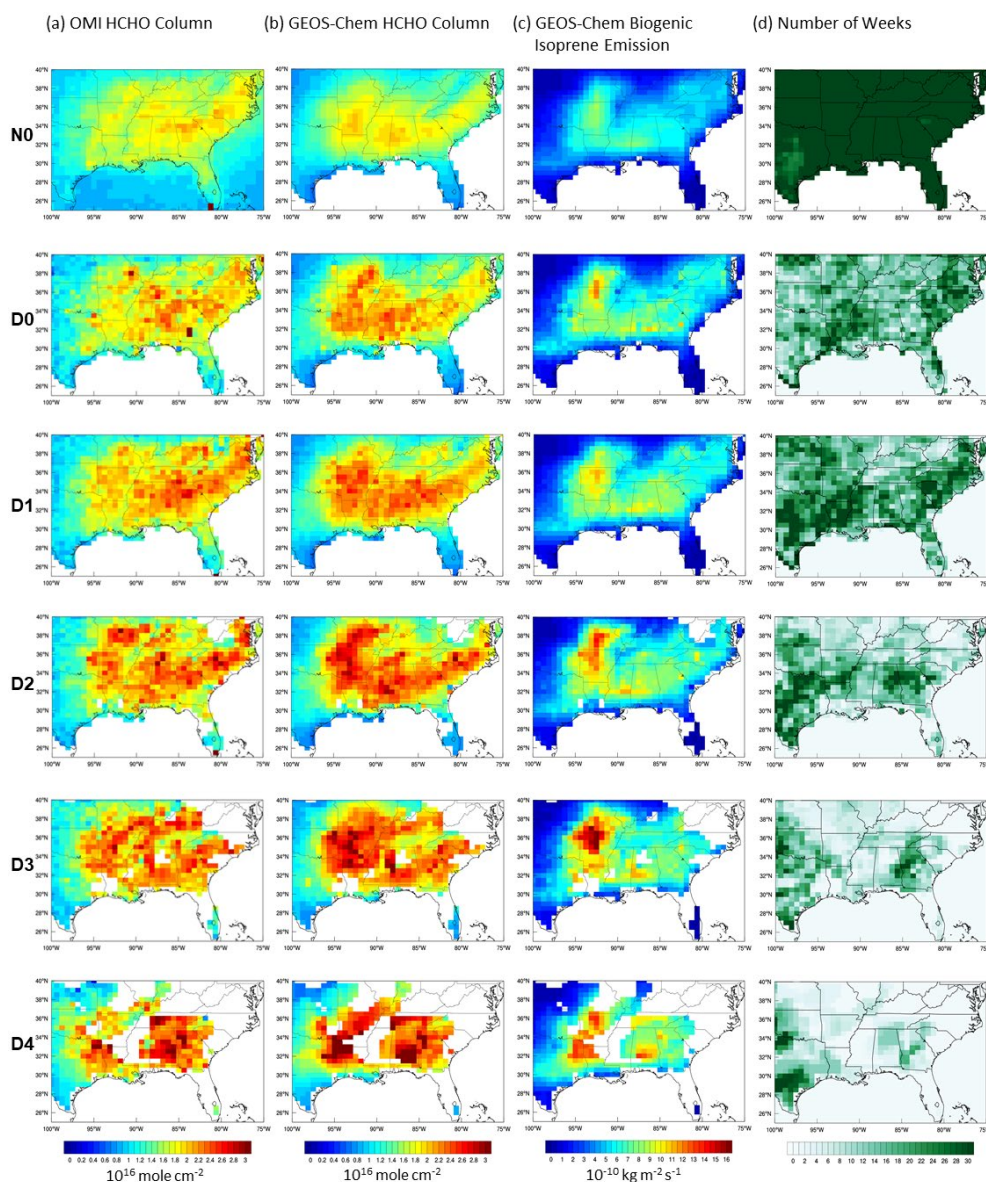
## 174 **3. Observational Evidence of Drought Stress on Isoprene Emissions**

### 175 **3.1 Changes of HCHO column densities with drought**

176 To reveal drought responses of HCHO, we sampled weekly-mean HCHO columns onto the gridded spatial and  
177 temporal locations of each USDM category and generated average HCHO distributions at each drought level over the  
178 SE US. The outputs are shown in **Figure 3a** for OMI and **3b** for NoStress\_GC, respectively. The processing of weekly-  
179 mean HCHO data corresponds to the timing of USDM: a whole week includes Wednesday of the previous week to  
180 Tuesday of the present week. There are 12 consecutive weeks from June to August in each year of 2005–2017, giving



181 a total of 156 weeks' gridded HCHO data to be assigned to individual USDM categories by week and location. **Figure**  
 182 **3d** shows the number of weeks underlying the gridded averages of HCHO for each USDM category. As severe  
 183 droughts are less frequent than mild droughts, some locations in SE US did not experience D2-D4 droughts during the  
 184 study period and hence are shown as white in **Figure 3**.



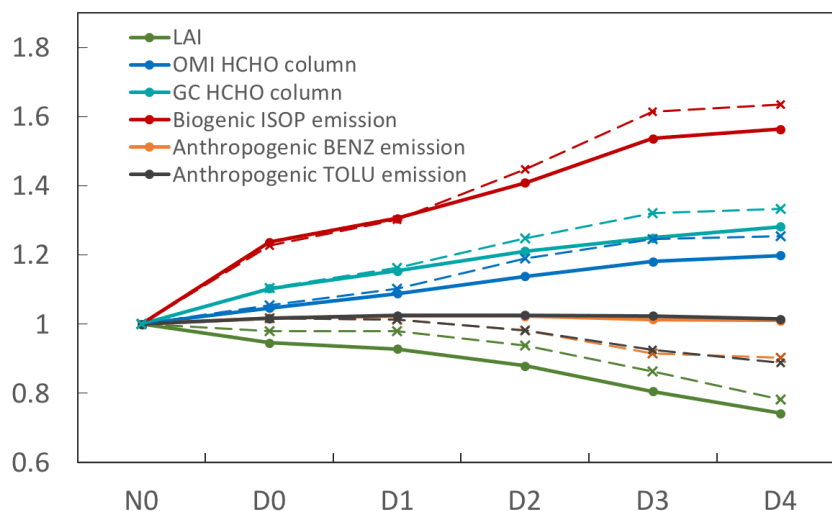
185

186 **Figure 3.** The mean spatial distributions of (a) OMI HCHO column density; (b) GEOS-Chem HCHO column density, (c)  
 187 isoprene emissions of NoStress\_GC, and (d) the number of weeks during JJA 2005 to 2017 in the southeast US under  
 188 different USDM drought levels (N0, D0-D4).



189 OMI HCHO column density increases with increasing drought severity in almost all locations in the SE US (**Figure**  
 190 **3a**). Relative to no-drought condition (N0), the mean HCHO column from OMI is 5.3%, 9.7%, 15.3%, 18.7%, and  
 191 19.8% higher under D0 - D4 drought in the entire SE US, respectively. These HCHO changes are statistically  
 192 significant at a 95% confident interval, indicating that the OMI HCHO products contain significant drought signals.  
 193 The rate of increase of OMI HCHO with USDM is not linear, faster under mild droughts (D0-D2) and flattening under  
 194 more severe droughts (D2-D4). This is qualitatively consistent with the conceptualized model of the nonlinear  
 195 response of isoprene emissions to drought described before (Potosnak et al., 2014).

196 Model HCHO column density also increases with increasing drought severity (**Figure 3b**). GCHCHO\_NoStress is  
 197 10.5%, 15.7%, 21.7%, 25.8%, and 28.9% higher under D0-D4 drought than that of N0, respectively. These increases  
 198 are 1.4-2.0 times those of OMI under all drought levels, and the rate of change in the model is more linear than OMI,  
 199 flattening only from D3 to D4. The model comparison against OMI HCHO also changes with drought severity.  
 200 GCHCHO\_NoStress has a minimal bias ( $0.06 \times 10^{16}$  mole  $\text{cm}^{-2}$ ) under N0. As drought severity increases, the mean  
 201 bias over the entire SE US increases to  $0.15 \times 10^{16}$  mole  $\text{cm}^{-2}$ ,  $0.14 \times 10^{16}$  mole  $\text{cm}^{-2}$ ,  $0.16 \times 10^{16}$  mole  $\text{cm}^{-2}$ ,  $0.18 \times$   
 202  $10^{16}$  mole  $\text{cm}^{-2}$ , and  $0.21 \times 10^{16}$  mole  $\text{cm}^{-2}$  under D0 - D4 levels, respectively. The spatial correlation between OMI  
 203 and NoStress\_GC degrades with USDM, with  $R^2$  being smaller than 0.7 under D0 - D4 levels compared to  $R^2$  of 0.87  
 204 under N0. Worsening model performance with increasing drought severity suggests the model lacks a process that  
 205 changes with drought. As isoprene accounts for more than 80% of the contribution of non-methane VOCs to the  
 206 HCHO column in the southeast US (Palmer et al., 2003; Millet et al., 2006), the missing process is most likely drought-  
 207 induced changes in isoprene emissions.



208

209 **Figure 4. Relative changes of regional-mean OMI HCHO column and GEOS-Chem (GC) simulated isoprene emissions**  
 210 **(red), anthropogenic benzene emission (orange), anthropogenic toluene emission (gray), and MODIS leaf area index (LAI,**  
 211 **green) under different drought levels in the southeast US. All data are scaled to their respective values at N0. The dotted**  
 212 **lines are the arithmetic mean of all grids, and the solid lines are the corrected mean excluding the missing area.**





213 **Figure 4** displays the relative changes in the regional mean HCHO column from OMI and NoStress\_GC, emissions  
214 of isoprene and select anthropogenic VOCs from NoStress\_GC, and MODIS LAI as a function of USDM indices,  
215 each scaled by its respective value at N0. The dotted line is the arithmetic mean of all available grids under each  
216 dryness category, and the solid line is the mean for those grids with valid data in all dryness categories (i.e., removing  
217 white areas shown in Figure 3). In either calculation, NoStress\_GC overestimates the relative increase of HCHO under  
218 D0-D4 by 40-100% compared to OMI. After correcting for no data areas at D2-D4, isoprene emissions in  
219 NoStress\_GC are 22.7%, 29.6%, 40.3%, 54.5%, and 56.0% higher in D0-D4 than N0. Note that LAI is observed to  
220 decrease by 5-10% per USDM level (**Figure 4**), which makes the predicted increase of isoprene emissions with  
221 drought severity even more remarkable.

222 By comparison, the modeled increase of the HCHO column with drought is 10-28%, more buffered than that of  
223 isoprene emissions. This is because HCHO depends not only on isoprene emissions but also on the abundance of  
224 oxidants, such as hydroxyl radicals (OH), that oxidize isoprene. High isoprene emissions can suppress OH under the  
225 low-NO<sub>x</sub> conditions that prevail in SE US (Wells et al., 2020), leading to the buffered response in HCHO. Given this  
226 suppression effect and the large increase of isoprene emissions in the model, the overestimation of HCHO columns  
227 by the model is unlikely to be caused by overestimating the oxidation rate of isoprene or other VOCs to HCHO, and  
228 more likely by the overestimation of isoprene emissions under drought conditions.

229 While oxidation of anthropogenic VOCs also produces HCHO, using benzene and toluene as indicator species, we  
230 found no change in anthropogenic VOC emissions with drought in the model (**Figure 4**). This insensitivity rules out  
231 anthropogenic VOCs as a key driver of model overestimation of HCHO under drought conditions. If anything, we  
232 expect anthropogenic VOC emissions to increase during drought due to higher evaporative emissions driven by higher  
233 temperature and more fossil fuel consumption driven by more demand for space cooling.

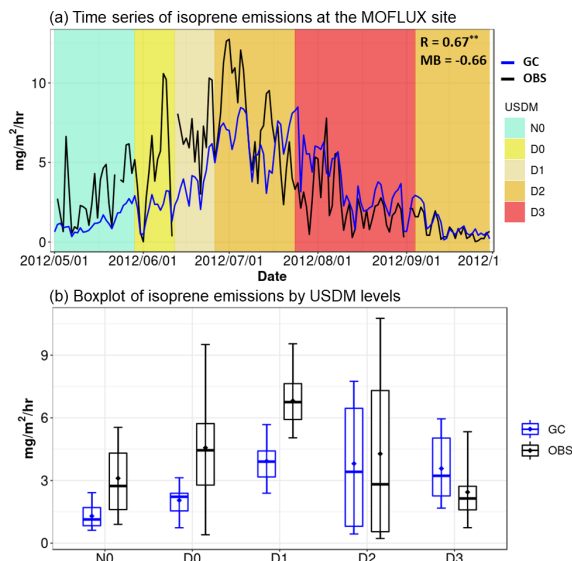
234 In summary, the model overestimates HCHO increases during drought as compared to OMI. This overestimation is  
235 attributed to the model overestimation of isoprene emissions during drought. Drought stress effect on isoprene  
236 emissions is thus required in GEOS-Chem to resolve the discrepancy in HCHO responses to drought between OMI  
237 and the model.

### 238 **3.2 Isoprene flux measurement**

239 To further evaluate isoprene emissions in NoStress\_GC, we compared the isoprene flux measurements at the  
240 MOFLUX site (Potosnak et al., 2014; Seco et al., 2015) with predicted isoprene emissions at the model grid that  
241 contains the site. At the time of writing, the MOFLUX site is the only long-term, canopy-level, biogenic isoprene flux  
242 measurement site in the Northern midlatitude that sampled droughts. The site experienced multiple drought levels in  
243 the summer of 2012, which allows for the model-observation comparison across different drought severities as shown  
244 in **Figure 5**. The abnormal dry conditions (D0) started in early June, which developed to moderate drought (D1) in  
245 late June, worsened to severe drought (D2) and extreme drought (D3) in July-August, and bounced back to D2 in  
246 September (**Figure 5a**). The model generally captures the daily variability of isoprene emissions with a statistically



247 significant correlation coefficient (R) of 0.67, but its biases differ by USDM levels. The model underestimates isoprene  
 248 flux from N0 (bias of -1.81 mg/m<sup>2</sup>/hr) to D1 (bias of -2.89 mg/m<sup>2</sup>/hr), has a minimal bias (-0.47 mg/m<sup>2</sup>/hr) at D2, and  
 249 changes to an overestimate at D3 (bias of 1.2 mg/m<sup>2</sup>/hr) (**Figure 5b**). While differences are expected when comparing  
 250 a single-point flux measurement with the grid-mean model prediction, such differences most likely result in a  
 251 systematic bias that should not relate to the temporal variability of drought. The fact that the model bias changes from  
 252 being underpredicting to overpredicting as drought severity increases further confirms the importance of the model  
 253 lack of a drought suppression effect on isoprene emissions during severe to exceptional droughts (D3 and D4). This  
 254 is qualitatively consistent with that of the HCHO biases described above.



255

256 **Figure 5. (a) Comparison of daily time series of isoprene emissions observed at the MOFLUX site (OBS) and simulated by**  
 257 **MEGAN2.1 in GEOS-Chem (GC). The background is color-coded according to the USDM drought severity. R and MB at**  
 258 **the upright corner show the correlation coefficient and mean bias, respectively. (b) Boxplot of isoprene emissions separated**  
 259 **by USDM drought levels. The upper and lower whiskers represent the 90% and 10% quantiles, respectively.**

#### 260 4. Drought Stress Algorithm

261 The MEGAN2.1 isoprene emission routines in GEOS-Chem use a simplified mechanistic representation of the major  
 262 environmental factors controlling biogenic emissions (Guenther et al., 2012), in which the isoprene emission factor  
 263  $\gamma_{2.1}$  is the product of a canopy-related normalization factor ( $C_{FAC}$ ) multiplied by other factors representing light ( $\gamma_{PAR}$ ),  
 264 temperature ( $\gamma_T$ ), leaf age ( $\gamma_{AGE}$ ), LAI ( $\gamma_{LAI}$ ), carbon dioxide ( $CO_2$ ) inhibition ( $\gamma_{CO_2}$ ), and soil moisture ( $\gamma_{SM}$ ):

$$265 \gamma_{2.1} = C_{FAC} \gamma_{PAR} \gamma_T \gamma_{AGE} \gamma_{LAI} \gamma_{CO_2} \gamma_{SM} = \gamma_0 \gamma_{SM} \quad (1)$$

266 where  $\gamma_0$  is the product of the non-drought factors. Because of the lack of reliable soil moisture databases,  $\gamma_{SM}$  is  
 267 always set to be one in GEOS-Chem as in many other chemical transport models, which means no water stress term



268 in the standard model configuration (i.e., NoStress\_GC). We show above that NoStress\_GC overestimates isoprene  
269 emissions and consequently HCHO column densities under drought conditions in the SE US. In this section, we  
270 describe the approach whereby observational constraints from the MOFLUX isoprene flux measurement and OMI  
271 HCHO were separately used to derive a drought stress factor  $\gamma_d$  which replaces  $\gamma_{SM}$  in Equation (1) to simulate the  
272 response of isoprene emissions to drought in MEGAN2.1 implementation of GEOS-Chem (hereafter referring to as  
273 GC/MEGAN2.1). The drought stress factor  $\gamma_d$  derived from the MOFLUX isoprene flux measurement is denoted as  
274  $\gamma_{d\_MOFLUX}$  and that from OMI HCHO as  $\gamma_{d\_OMI}$ . Their corresponding simulations are referred to as  
275 MOFLUX\_Stress\_GC and OMI\_Stress\_GC, respectively.

#### 276 4.1 MOFLUX-based Drought Stress Algorithm

277 The  $\gamma_{d\_MOFLUX}$  was derived following Jiang et al. (2018) by implementing photosynthesis and water stress parameters  
278 with a formula of:

$$279 \quad \gamma_{d\_MOFLUX} = \gamma_0 \gamma_{d\_isoprene} \begin{cases} \gamma_{d\_isoprene} = 1 (\beta_t \geq 0.3) \\ \gamma_{d\_isoprene} = V_{cmax}/\alpha (\beta_t < 0.3, \alpha = 77) \end{cases} \quad (2)$$

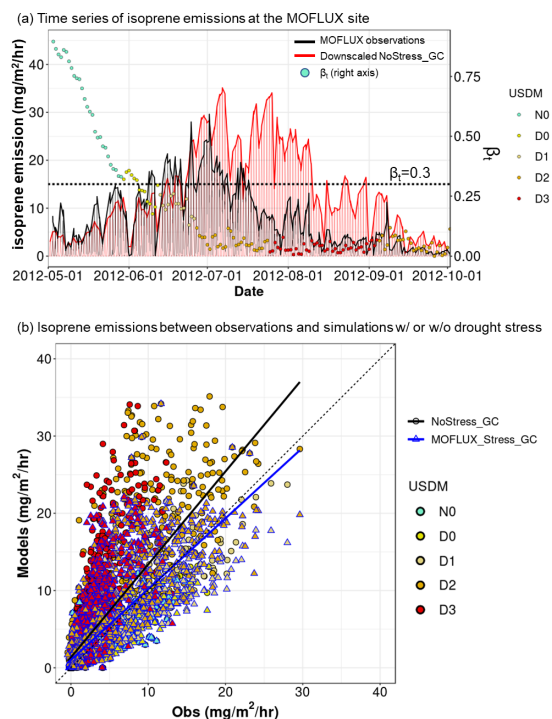
280 Where  $V_{cmax}$  is the maximum carboxylation rate by photosynthetic Rubisco enzyme and  $\beta_t$  represents the water stress  
281 ranging from zero (fully stressed) to one (no stress). This simplified method intends to use the decreased  
282 photosynthetic enzyme activity to physiologically represent the variation in isoprene emissions under drought stress  
283 via dividing  $V_{cmax}$  by an empirical parameter  $\alpha$  when the water stress is below a threshold.

284 Since the default GEOS-Chem does not have these photosynthetic parameters, we adopted the ecophysiology module  
285 created by Lam and Tai (submitted) that is based on the photosynthesis calculation in the Joint UK Land  
286 Environmental Simulator (JULES; Best et al., 2011; Clark et al., 2011) as an online component in GEOS-Chem so  
287 that it simulates photosynthesis rate and bulk stomatal conductance dynamically and consistently with the underlying  
288 meteorology that drives GEOS-Chem. The outputs of  $V_{cmax}$  and  $\beta_t$  from the ecophysiology module were passed to  
289 MEGAN2.1 in GEOS-Chem to parameterize the drought stress according to Equation 2. In addition to GEOS-Chem  
290 meteorology, the ecophysiology module uses soil parameters from the Hadley Centre Global Environment Model  
291 version 2 – Earth System Model (HadGEM2-ES). In general, the implementation of the ecophysiology module much  
292 improved the simulated stomatal conductance and dry deposition velocity relative to site observations on average for  
293 seasonal timescales, but the  $\beta_t$  computed has not been calibrated to intermittent drought conditions. Instead of adopting  
294 the values of  $V_{cmax}$  and  $\beta_t$  from Jiang et al. (2018) which were based on the Community Land Model, we need to  
295 determine the  $\beta_t$  threshold and the  $\alpha$  value specific to GEOS-Chem with the ecophysiology module of Lam and Tai  
296 (submitted). To calibrate  $\beta_t$ , we first examined the statistical distribution of  $\beta_t$  at the MOFLUX grid (**Figure S1**) during  
297 May-September 2011 and 2012 when multiple USDM drought categories occurred. Then we decided on a value of  
298 0.3 as the threshold  $\beta_t$  below which the drought stress will be triggered in the model because this value is greater than  
299 75% quantile of all the  $\beta_t$  values from D0 to D3, thus capturing most of the drought conditions.



300 We note the observed isoprene flux at MOFLUX is consistently higher than predicted values during the non-drought  
 301 period (e.g., N0 in Figure 5a). This systematic bias is expected because we compare the single-point observations with  
 302 grid-mean isoprene emission fluxes. To correct the systemic bias, we scaled down the model isoprene emissions at  
 303 the MOFLUX grid by a factor of 1.42, which eliminated the mean bias of the hourly simulated and observed isoprene  
 304 fluxes at the MOFLUX grid during non-drought conditions ( $\beta_t > 0.3$ ). The factor of 1.42 was applied to downscale  
 305 modeled isoprene fluxes at the MOFLUX grid during the entire time series, including drought conditions. The resulted  
 306 time series are shown in **Figure 6a**. Based on the downscaled model prediction, we derived that  $\alpha=77$  under drought  
 307 conditions ( $\beta_t < 0.3$ ), which minimized the mean bias under drought conditions between the modeled and observed  
 308 isoprene fluxes at the MOFLUX grid.

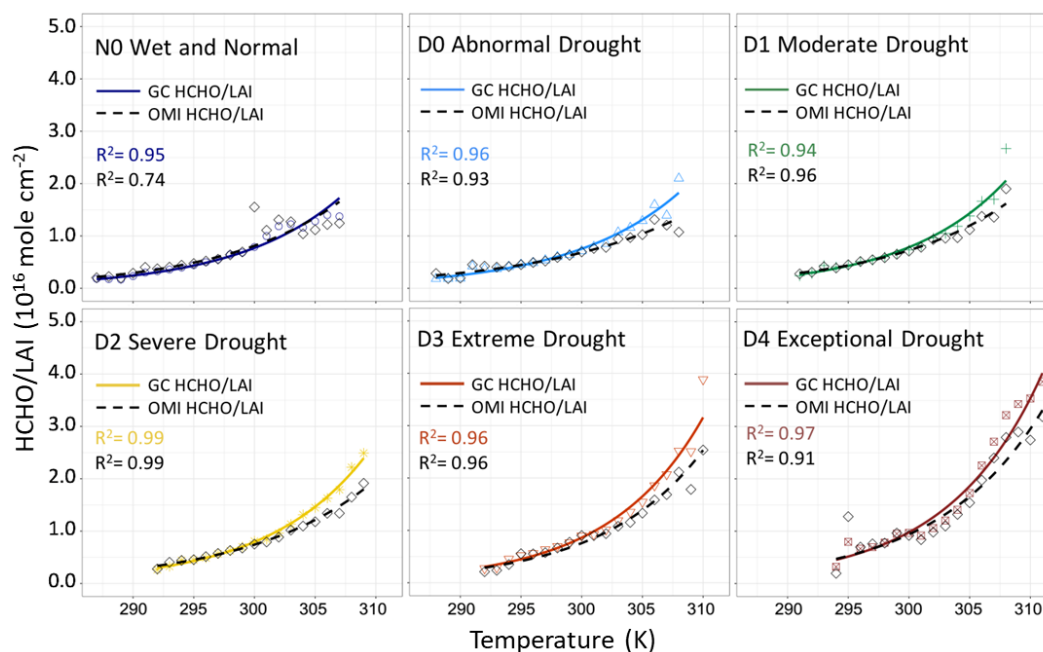
309 **Figure 6b** shows the comparison of the hourly NoStress\_GC and MOFLUX\_Stress\_GC isoprene emissions with  
 310 observations in May-September 2012. The overall mean bias is reduced from 2.05 mg/m<sup>2</sup>/hr to 0.01 mg/m<sup>2</sup>/hr despite  
 311 the fact that the stress factor is only applied to drought conditions. The correlation coefficient (R) and index of  
 312 agreement (IOA) also increase from 0.77 to 0.85 and from 0.80 to 0.93, respectively. All the changes in the comparison  
 313 metrics indicate the model simulations are improved considerably based on the single-point measurement.



314  
 315 **Figure 6. (a)** Observed (black line) and simulated (red line; after downscaling) hourly time series of isoprene emissions at  
 316 the MOFLUX site. The dots color-coded by USDM levels represent the daily values of  $\beta_t$  (right axis). The dashed line  
 317 indicates the threshold of 0.3. **(b)** Comparison of isoprene emissions between observations (Obs) and simulations with  
 318 (MOFLUX\_Stress\_GC; blue-bordered triangle) and without (NoStress\_GC; black-bordered circle) drought stress. Data  
 319 are color-coded by USDM levels.



320 **4.2 OMI-based Drought Stress Algorithm**



321

322 **Figure 7. Response of HCHO/LAI ratio ( $10^{16}$  mole  $\text{cm}^{-2}$ ) to temperature (K) in different drought levels averaged over JJA**  
 323 **2005-2017. The colored solid line is the modelled NoStress\_GC HCHO/LAI ratio, and the black dashed line is the observed**  
 324 **HCHO/LAI ratio from OMI. The exponentially fitted formulas and the resulted coefficient of determination ( $R^2$ ) are**  
 325 **labelled in each subplot.**

326 Isoprene emission increases exponentially with temperatures below  $\sim 310$  K (Guenther et al., 2006) in the absence of  
 327 other stress factors such as drought. Indeed, an exponential relationship between biogenic isoprene emission per unit  
 328 LAI and temperature is predicted by MEGAN2.1 at all USDM levels (**Figure S2**). However, the predicted temperature  
 329 sensitivity is found to increase substantially with drought severity with no sign of plateauing or slow-down even under  
 330 the most severe drought conditions when MOFLUX measurements measured a decrease in isoprene emissions (c.f.  
 331 Figure 5). Similarly, we found NoStress\_GC overestimates HCHO sensitivities to high temperatures ( $> 300$  K) under  
 332 drought conditions (D0-D4) (**Figure 7**), but no such overestimation is seen under non-drought (N0) or low temperature  
 333 conditions during drought ( $< 300$  K). This indicates the role of drought stress on isoprene emissions is likely through  
 334 suppressing the dependence of emissions on temperatures during drought. Leaf level measurements conducted during  
 335 the 2012 drought at the MOFLUX site provide independent evidence of drought suppression of the isoprene response  
 336 to increasing temperature for less drought-resilient tree species (Geron et al., 2016). Taking advantage of these  
 337 empirical observations, we derived the OMI-based drought stress algorithm by minimizing the differences in HCHO  
 338 column sensitivities to temperatures between OMI and GEOS-Chem under drought conditions as shown in Figure 7.  
 339 When calculating the relationships between HCHO column densities and temperatures, we first scaled HCHO column  
 340 by LAI on a grid-by-grid basis to account for the regional differences in isoprene emissions due to different vegetation  
 341 coverage as well as the effect of LAI changes with drought (c.f. **Figure 4**). Each point in **Figure 7** represents the mean



342 HCHO/LAI ratio, denoted as  $\Omega$ , within each 1K temperature interval. We used exponential functions ( $\ln\Omega = kT + b$ ) to  
 343 separately fit the temperature (T) dependence of HCHO/LAI ratio ( $\Omega$ ) under different drought levels (**Figure 7**) for  
 344 both the model and OMI. The resulted formulas were listed in **Table 1** and the  $R^2$  of most fitting lines is greater than  
 345 0.9.

346 **Table 1. Fitted exponential formulas of GC and OMI HCHO/LAI ratio ( $\Omega$ ,  $10^{16}$  mole  $\text{cm}^{-2}$ ) to surface air temperature (T,  
 347 K), and fitted value of HCHO/LAI ratio at 290K, 300K, and 310K.**

USDM	GC HCHO/LAI ( $\Omega$ , $10^{16}$ mole $\text{cm}^{-2}$ )				OMI HCHO/LAI ( $\Omega$ , $10^{16}$ mole $\text{cm}^{-2}$ )			
	Fitting Formula	290K	300K	310K	Fitting Formula	290K	300K	310K
N0	$\ln\Omega = 0.115T - 34.73$	0.24	0.77	2.43*	$\ln\Omega = 0.101T - 30.66$	0.29	0.81	2.24*
D0	$\ln\Omega = 0.110T - 33.43$	0.25	0.75	2.27	$\ln\Omega = 0.085T - 25.80$	0.29	0.68	1.59
D1	$\ln\Omega = 0.121T - 36.43$	0.23	0.78	2.62	$\ln\Omega = 0.100T - 30.44$	0.27	0.72	1.98
D2	$\ln\Omega = 0.123T - 36.99$	0.23	0.79	2.70	$\ln\Omega = 0.098T - 29.84$	0.28	0.74	1.99
D3	$\ln\Omega = 0.130T - 39.11$	0.23	0.86	3.16	$\ln\Omega = 0.121T - 36.50$	0.28	0.76	2.53
D4	$\ln\Omega = 0.128T - 38.55$	0.27	0.98	3.54	$\ln\Omega = 0.115T - 34.49$	0.30	0.93	2.95

348 \* Asterisk indicates that the temperature does not reach this value in actual data and is an extrapolated value.

349 As the fitting equations suggest, both GEOS-Chem and OMI HCHO/LAI ratios increase with temperature under all  
 350 conditions, but the former shows a higher sensitivity to temperature under drought conditions. This can be clearly seen  
 351 from the higher HCHO/LAI ratios of GEOS-Chem ( $\Omega_{GC}$ ; solid lines) than those of OMI ( $\Omega_{OMI}$ ; dashed lines) especially  
 352 when the temperature is greater than 300 K under D0-D4. To better explain this, we also calculated the fitted value of  
 353 HCHO/LAI at three temperatures of 290K, 300K, and 310K in **Table 1**. Since it is difficult for the N0 condition to  
 354 reach a temperature of 310K, the values were extrapolated and marked with an asterisk in the table. The results show  
 355 that the model overestimates the temperature dependence at all drought levels. At 290K, all biases between  $\Omega_{OMI}$  and  
 356  $\Omega_{GC}$  are less than  $0.05 \times 10^{16}$  mole  $\text{cm}^{-2}$ . At 310K, the bias between the two is  $0.19 \times 10^{16}$  mole  $\text{cm}^{-2}$  (8.5%) at N0 but  
 357 increases by more than a factor of 3 to  $0.68 \times 10^{16}$  mole  $\text{cm}^{-2}$  (42.8%),  $0.64 \times 10^{16}$  mole  $\text{cm}^{-2}$  (32.3%),  $0.71 \times 10^{16}$   
 358 mole  $\text{cm}^{-2}$  (35.7%),  $0.63 \times 10^{16}$  mole  $\text{cm}^{-2}$  (24.9%), and  $0.59 \times 10^{16}$  mole  $\text{cm}^{-2}$  (20.0%) at D0-D4 drought, respectively.  
 359 Based on the fitted formulas in **Table 1**, the ratio between  $\frac{\Omega_{OMI}}{\Omega_{GC}}$  under each level from D0 to D4 can be derived by:

$$360 \quad \frac{\Omega_{OMI}}{\Omega_{GC}} = \frac{e^{k_{OMI}T + b_{OMI}}}{e^{k_{GC}T + b_{GC}}} = e^{(k_{OMI} - k_{GC})T} e^{(b_{OMI} - b_{GC})} \quad (3)$$



361 where  $k_{OMI}$  ( $k_{GC}$ ) and  $b_{OMI}$  ( $b_{GC}$ ) represent the slopes and interpolations of the formulas in **Table 1** for OMI (GC)  
 362 HCHO column; T is surface temperature, and e is the exponential constant. By averaging the values of  $k_{OMI}$ - $k_{GC}$  and  
 363  $b_{OMI}$ - $b_{GC}$  from D0 to D4, we can obtain:

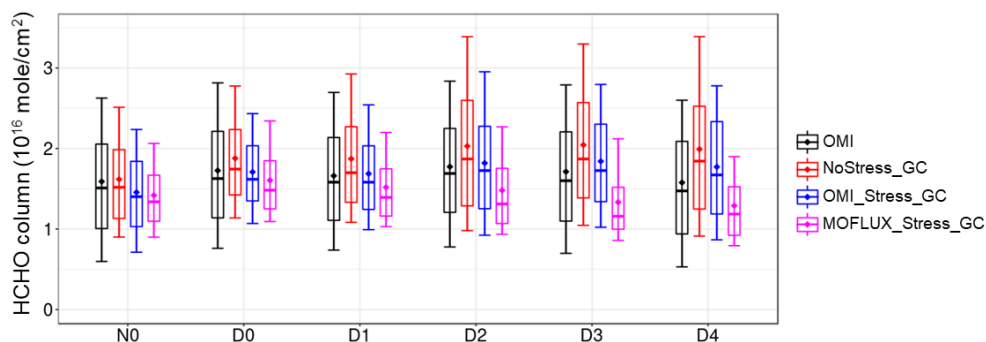
$$364 \frac{\Omega_{OMI}}{\Omega_{GC}} = 383.38e^{-0.02T} (\beta_t < 0.6, T > 300 K) \quad (4)$$

365 where  $\beta_t < 0.6$  represents the 75% quantile of the  $\beta_t$  values from D0 to D4 for the whole SE US study region in JJA  
 366 2005-2017 (**Figure S1**).

367 The formula of  $\gamma_{d\_OMI}$  is thus:

$$368 \gamma_{d\_OMI} = \gamma_0 \gamma_{d\_isoprene} \begin{cases} \gamma_{d\_isoprene} = 1 (\beta_t \geq 0.6 \text{ or } T \leq 300K) \\ \gamma_{d\_isoprene} = \frac{\Omega_{OMI}}{\Omega_{GC}} = 383.38e^{-0.02T} (\beta_t < 0.6, T > 300K) \end{cases} \quad (5)$$

369 Note the threshold of  $\beta_t$  in equation 5 is different from the value used by  $\gamma_{d\_MOFLUX}$  because all the SE US grids were  
 370 considered in deriving  $\beta_t$  for  $\gamma_{d\_OMI}$ . Another difference is that the factor is activated only if the temperature is higher  
 371 than 300K when significant biases between  $\Omega_{OMI}$  and  $\Omega_{GC}$  are found (**Figure 7**).



372

373 **Figure 8.** Boxplot of HCHO column statistical distributions for OMI observations (black) and different GEOS-Chem  
 374 simulations: without drought stress (NoStress\_GC; red) and with drought stress factors derived from MOFLUX  
 375 observations (MOFLUX\_Stress\_GC; blue) and from OMI HCHO constraints (OMI\_Stress\_GC; pink).

376 **Figure 8** compares the statistical distributions of HCHO column densities from OMI, NoStress\_GC,  
 377 MOFLUX\_Stress\_GC, and OMI\_Stress\_GC during May-September 2012 over the SE US. Compared to OMI,  
 378 NoStress\_GC simulation has a mean high bias of  $0.15 \times 10^{16}$  mole  $\text{cm}^{-2}$  -  $0.42 \times 10^{16}$  mole  $\text{cm}^{-2}$  during D0-D4. The  
 379  $\gamma_{d\_OMI}$  algorithm reduces the high bias to  $0.02 \times 10^{16}$  mole  $\text{cm}^{-2}$  -  $0.20 \times 10^{16}$  mole  $\text{cm}^{-2}$ . By contrast, the  $\gamma_{d\_MOFLUX}$   
 380 algorithm reduces the HCHO simulations too much over the SE US and causes an overall underestimation of  $0.12 \times 10^{16}$   
 381 mole  $\text{cm}^{-2}$  -  $0.38 \times 10^{16}$  mole  $\text{cm}^{-2}$ . The  $\gamma_{d\_MOFLUX}$  algorithm also narrows the statistical distribution of HCHO as  
 382 indicated by the smaller boxes and shorter whiskers compared to OMI. This suggests that the  $\gamma_{d\_MOFLUX}$  algorithm  
 383 based on the single-site observations is incapable of representing the drought stress over the SE US. Thus, the  $\gamma_{d\_OMI}$



384 algorithm is used in the next section to further evaluate how this algorithm would change the responses of atmospheric  
385 compositions to droughts.

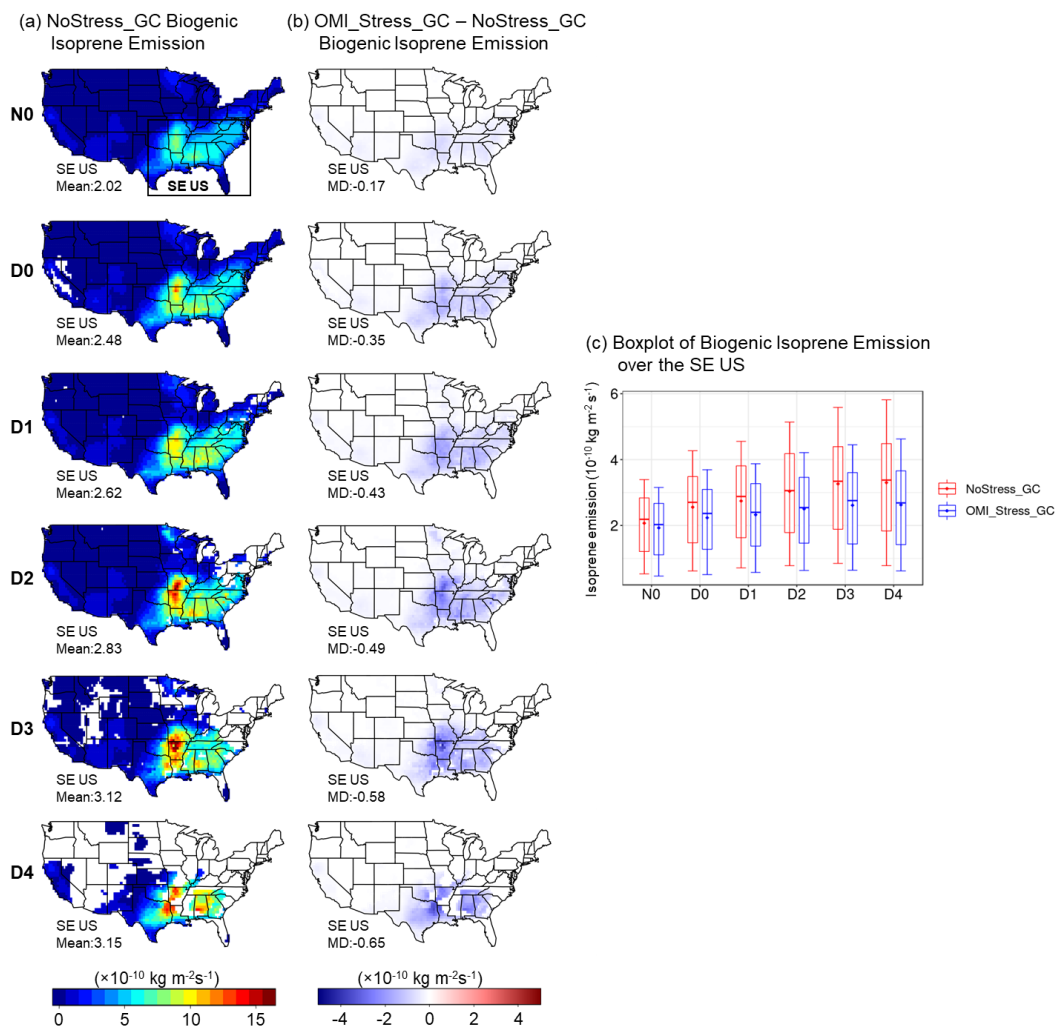
### 386 5. Changes in Simulated Biogenic Isoprene Emissions, HCHO, O<sub>3</sub>, and OA

387 In this section, we evaluated the changes in biogenic isoprene emissions and HCHO column densities by running a  
388 long-term (2005-2017, JJA) simulation, after adding the OMI-based drought stress factor for isoprene emissions  $\gamma_{d\_OMI}$   
389 in GEOS-Chem. Since isoprene is an important precursor for the formation of tropospheric O<sub>3</sub> and OA, maximum  
390 daily 8-hour average (MDA8) O<sub>3</sub>, and OA changes were also examined. We used the ComplexSOA mechanism in  
391 GEOS-Chem (Pye et al., 2010; Marais et al., 2016) which includes more detailed pathways of isoprene to secondary  
392 organic aerosols such as aqueous-phase reactive uptake and the formation of organo-nitrates.

393 **Figure 9** shows the changes in biogenic isoprene emissions resulting from adding  $\gamma_{d\_OMI}$  drought stress in GEOS-  
394 Chem. Here we expanded the maps to the entire contiguous US to examine whether the drought stress algorithm can  
395 impose large changes on other US regions although it is derived based on the SE US data only. The numbers at each  
396 panel indicate the means of isoprene emissions of NoStress\_GC and the mean differences (MD) relative to the  
397 OMI\_Stress\_GC over the SE US. As expected, the biggest decrease in isoprene emissions is found in the SE US with  
398 the regional-mean emissions reduced by  $0.17 \times 10^{-10} \text{ kg m}^{-2} \text{ s}^{-1}$  (8.60%),  $0.35 \times 10^{-10} \text{ kg m}^{-2} \text{ s}^{-1}$  (14.24%),  $0.43 \times 10^{-10} \text{ kg}$   
399  $\text{m}^{-2} \text{ s}^{-1}$  (16.57%),  $0.49 \times 10^{-10} \text{ kg m}^{-2} \text{ s}^{-1}$  (17.49%),  $0.58 \times 10^{-10} \text{ kg m}^{-2} \text{ s}^{-1}$  (18.66%), and  $0.65 \times 10^{-10} \text{ kg m}^{-2} \text{ s}^{-1}$  (20.74%)  
400 from N0 to D4, respectively (**Figure 9c**). Despite lowering emissions relative to NoStress\_GC, OMI\_Stress\_GC  
401 simulates an increase of isoprene emissions under drought conditions compared to non-drought in the SE US; the  
402 respective increases are  $0.28 \times 10^{-10} \text{ kg m}^{-2} \text{ s}^{-1}$  (15.20%),  $0.34 \times 10^{-10} \text{ kg m}^{-2} \text{ s}^{-1}$  (18.40%),  $0.49 \times 10^{-10} \text{ kg m}^{-2} \text{ s}^{-1}$  (26.47%),  
403  $0.69 \times 10^{-10} \text{ kg m}^{-2} \text{ s}^{-1}$  (37.46%), and  $0.65 \times 10^{-10} \text{ kg m}^{-2} \text{ s}^{-1}$  (35.23%) from D0 to D4 relative to N0 (**Figure 9c**). This  
404 increase results from the top-down constraints by the corresponding changes in OMI HCHO column densities with  
405 USDM and consequently exhibits the behavior of non-uniform increases with drought severity (e.g., peak increase of  
406 37.5% at D3, followed by a ~2% reduction at D4), which is consistent with the MOFLUX flux measurements.

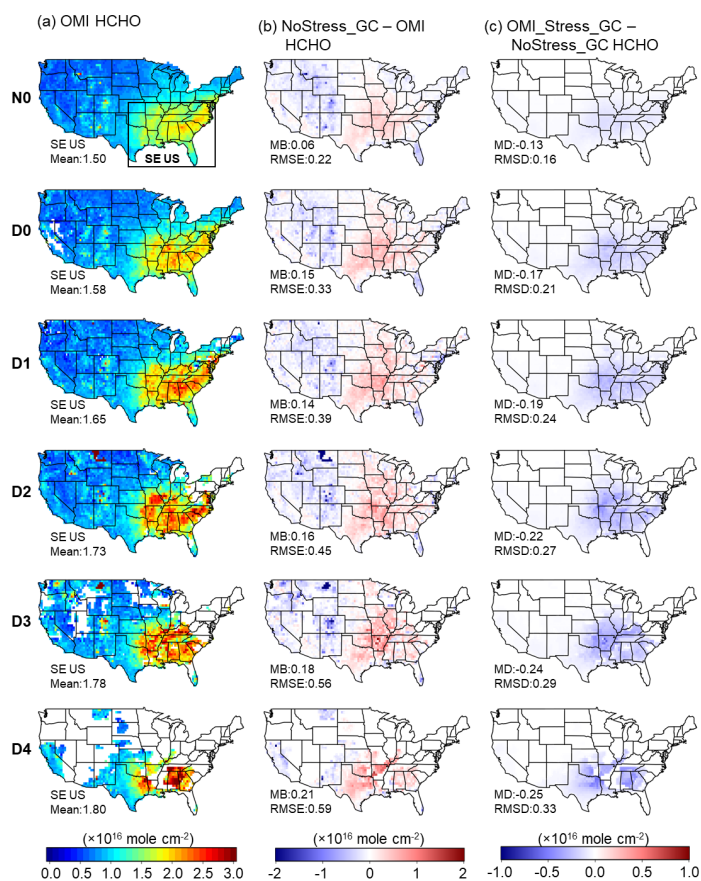
407 For other regions, such as California and Minnesota, biogenic isoprene emissions decreased slightly by less than  
408  $0.5 \times 10^{-10} \text{ kg m}^{-2} \text{ s}^{-1}$ . The smaller effect of the drought stress factor imposed on regions other than the SE US is  
409 understandable because of the lower isoprene emissions.





410

411 **Figure 9. Simulated biogenic isoprene emissions during JJA 2005-2017 by USDM dryness category by NoStress\_GC (a),**  
 412 **OMI\_Stress\_GC minus NoStress\_GC (b), and statistical distributions of SE US isoprene emissions between the two**  
 413 **simulations (c). Numbers at the bottom-left corner of each panel indicate the SE US (black box) regional mean of biogenic**  
 414 **isoprene emissions for NoStress\_GC (left column), and mean differences (MD) between OMI\_Stress\_GC and NoStress\_GC**  
 415 **(middle column).**



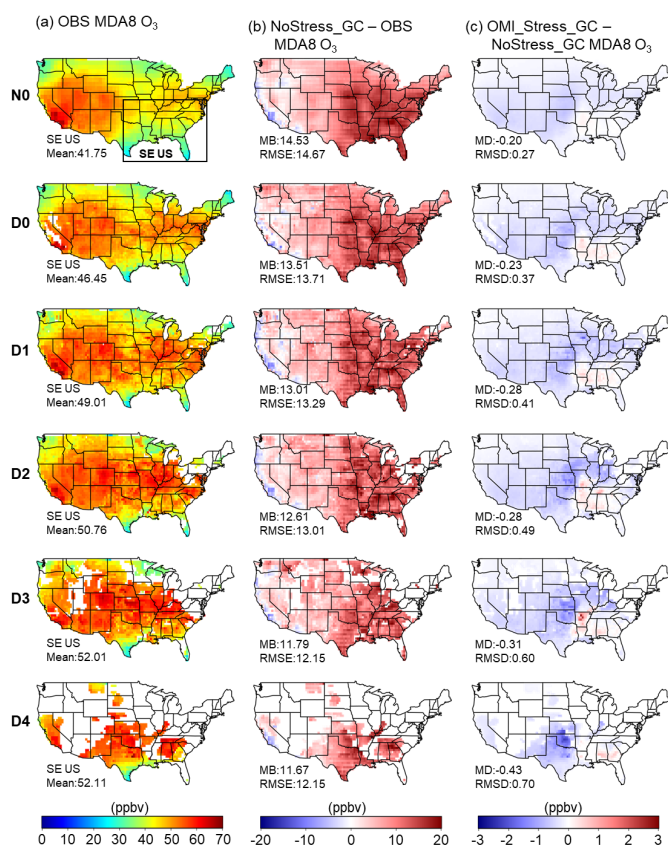
416

417 **Figure 10.** Mean HCHO column densities during JJA 2005-2017 by USDM dryness category for OMI (a), NoStress\_GC  
 418 minus OMI (b), and OMI\_Stress\_GC minus NoStress\_GC (c). Numbers at the bottom-left corner of each panel indicate the  
 419 SE US (black box) regional mean of OMI HCHO column (left column), mean bias (MB), and root mean square error  
 420 (RMSE) in HCHO column densities between NoStress\_GC and OMI (middle column), and mean differences (MD) and root  
 421 mean square deviation (RMSD) between OMI\_Stress\_GC and NoStress\_GC (right column). MD and RMSD are calculated  
 422 in the same way as MB and RMSE; the different names are used to distinguish between model-to-model comparison and  
 423 model-to-observation comparison, respectively.

424 The changes in the HCHO column are shown in **Figure 10**. Different from the overestimation in the SE US,  
 425 NoStress\_GC underestimates HCHO column densities in the western US compared to OMI (**Figure 10b**). This  
 426 negative bias should be interpreted with care because the scaling factor of 1.59 (c.f. section 2.2) is derived over the  
 427 SE US and may not hold in other regions. For the SE US overall, the drought stress factor reduces modeled HCHO  
 428 columns by  $0.17 \times 10^{16}$  mole  $\text{cm}^{-2}$  (9.82%),  $0.19 \times 10^{16}$  mole  $\text{cm}^{-2}$  (10.61%),  $0.22 \times 10^{16}$  mole  $\text{cm}^{-2}$  (11.64%) and  
 429  $0.24 \times 10^{16}$  mole  $\text{cm}^{-2}$  (12.24%),  $0.25 \times 10^{16}$  mole  $\text{cm}^{-2}$  (12.44%) under D0-D4, respectively, relative to NoStress\_GC  
 430 (**Figure 10c**). This leads to a better agreement with OMI as OMI\_Stress\_GC has nearly zero MB under D0-D4 (MB  
 431 =  $-0.02 \times 10^{16}$  mole  $\text{cm}^{-2}$  ~  $0.05 \times 10^{16}$  mole  $\text{cm}^{-2}$ ). The RMSE is also reduced by 18%-24% relative to the NoStress\_GC  
 432 simulation compared to observations (not shown). The changes in both metrics indicate that the drought algorithm



433 considerably improves the model performance in capturing the biogenic isoprene response to drought as evidenced by  
 434 HCHO column. Similar to the changes in biogenic isoprene emissions, the OMI\_Stress\_GC only slightly decreases  
 435 HCHO column densities (<5%) compared to the NoStress\_GC simulation in other US regions.



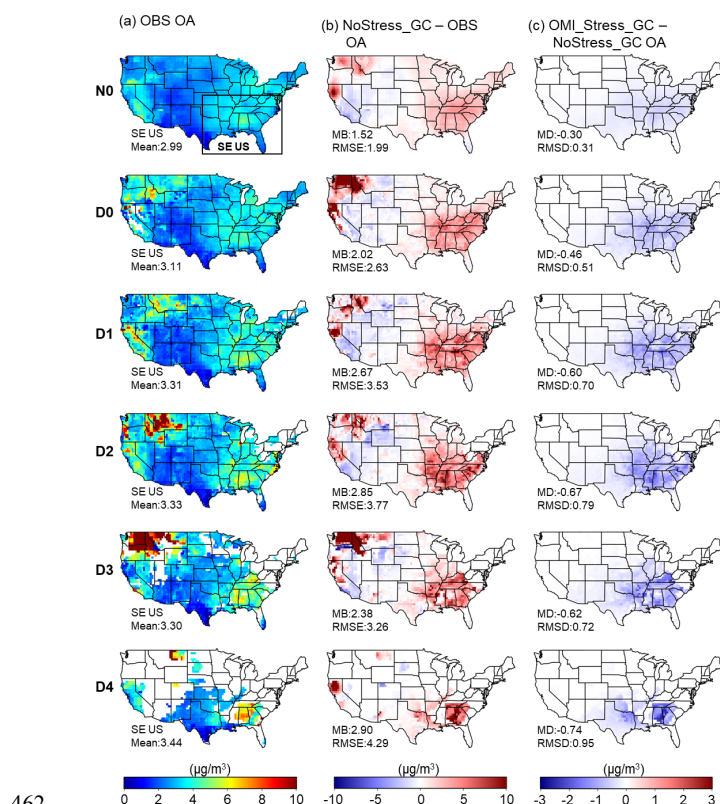
436

437 **Figure 11. Same as Figure 10 but for surface maximum daily 8-hour average (MDA8) O<sub>3</sub>.**

438 **Figure 11a** displays the observed MDA8 O<sub>3</sub> changes with USDM. Similar to the changes of the HCHO column with  
 439 USDM levels, O<sub>3</sub> in the SE US exhibits a gradual increase, relative to the mean of 41.74 ppbv at N0, of 4.70 ppbv,  
 440 7.26 ppbv, 9.01 ppbv, 10.26 ppb, and 10.36 ppbv under D0-D4, respectively. This is consistent with our previous  
 441 study (Li et al., 2022; Lei et al., 2022) which investigated O<sub>3</sub> changes with drought severity in more detail. The  
 442 NoStress\_GC simulation has a high bias in MDA8 O<sub>3</sub> across all USDM categories (**Figure 11b**). High positive bias  
 443 is a common issue of surface O<sub>3</sub> simulations in chemical transport models, which is a research question and can be  
 444 attributed to the uncertainties in various processes, such as NO<sub>x</sub> emissions, isoprene oxidation pathways, O<sub>3</sub> dry  
 445 deposition velocity, boundary layer dynamics (Fiore et al., 2005; Lin et al., 2008; Squire et al., 2015; Travis et al.,  
 446 2016; Travis and Jacob, 2019). Despite the systematic high bias, NoStress\_GC captures the increasing trend of MDA8  
 447 O<sub>3</sub> with increasing dryness but with a respectively smaller increment (relative to N0) of 3.62 ppbv, 5.67 ppbv, 7.01



448 ppbv, 7.41 ppbv, and 7.41 ppbv under D0 to D4. This discrepancy between NoStress\_GC and observations can also  
 449 be inferred from the fact that the MB between model and observations decreases from 14.53 ppbv at N0 to 11.67 ppbv  
 450 at D4 (**Figure 11b**). **Figure 11c** shows the difference in MDA8 O<sub>3</sub> between OMI\_Stress\_GC and NoStress\_GC. In  
 451 the SE US where isoprene emissions are the highest and reduced the most by the drought stress algorithm,  
 452 OMI\_Stress\_GC shows a small increase in MDA8 O<sub>3</sub> of less than 1 ppbv. This increase in O<sub>3</sub> can be explained by an  
 453 increase of OH resulting from reducing isoprene emissions under low-NO<sub>x</sub> conditions in the SE US (Wells et al.,  
 454 2020). For the SE US study domain as a whole, the change in MDA8 ozone was negligible but negative (regional  
 455 mean of -0.5 ppbv). Although the drought factor does not reduce the overall high bias, it makes the model more  
 456 consistent with the observed increment in MDA8 O<sub>3</sub> for the subregion with increased O<sub>3</sub> (e.g., 90–94°W, 32–35°N) as  
 457 drought severity increases. Over northeastern Texas, Oklahoma, and Kansas where isoprene emission is also reduced  
 458 by the drought algorithm yet from a much lower emission base compared to other SE US areas, OMI\_Stress\_GC  
 459 simulates 1-3 ppbv lower MDA8 O<sub>3</sub> under drought conditions (D0-D4), leading to a better agreement with  
 460 observations. For regions with lower isoprene and higher NO<sub>x</sub> concentrations, O<sub>3</sub> formation is more sensitive to the  
 461 changes in isoprene, which explains the reduction in MDA8 O<sub>3</sub> caused by the drought stress factor.



462

463 **Figure 12.** Same as Figure 10 but for organic aerosol (OA).



464 The changes in OA with USDM are shown in **Figure 12**. Observed OA in the SE US shows an average increase  
465 (relative to N0) of 0.12  $\mu\text{g}/\text{m}^3$ , 0.32  $\mu\text{g}/\text{m}^3$ , 0.34  $\mu\text{g}/\text{m}^3$ , 0.31  $\mu\text{g}/\text{m}^3$ , and 0.45  $\mu\text{g}/\text{m}^3$  under D0 to D4, respectively. The  
466 extremely high values over the northwest states (e.g., Washington and Montana) are likely associated with higher  
467 wildfire emissions under droughts (Wang et al., 2017). The NoStress\_GC simulation considerably overestimates OA  
468 in the SE US with an MB of 1.52  $\mu\text{g}/\text{m}^3$  (50.83%) at N0 and the overestimation becomes even higher to 2.02-2.90  
469  $\mu\text{g}/\text{m}^3$  (64.95%-85.58%) at D0-D4 (**Figure 12b**), thus causing an overprediction of the drought-OA relationship.  
470 Zheng et al (2020) reported a similar level of overestimation and attributed this to the overdependence of isoprene-  
471 derived secondary organic aerosol (SOA) on sulfate. As isoprene is one of the dominant sources of OA in the SE US  
472 (Xu et al., 2015; Budisulistiorini et al., 2016), our analysis suggests that the model overestimation of isoprene  
473 emissions under drought conditions is another reason for this high OA bias in the SE US. Indeed, the drought stress  
474 factor greatly improves the OA simulation by reducing the MB by 0.30  $\mu\text{g}/\text{m}^3$  (6.60%), 0.46  $\mu\text{g}/\text{m}^3$  (8.98%) 0.60  
475  $\mu\text{g}/\text{m}^3$  (10.07%), 0.67  $\mu\text{g}/\text{m}^3$  (10.85%), 0.62  $\mu\text{g}/\text{m}^3$  (10.88%), 0.74  $\mu\text{g}/\text{m}^3$  (11.71%) under N0 to D4 over the SE US  
476 relative to NoStress\_GC, thus lowering the MB to be within 1.22-2.18  $\mu\text{g}/\text{m}^3$  (40.82% - 65.52%) compared with  
477 observations. We also examined the change of three major SOA components in **Figure S3**. Anthropogenic SOA  
478 (ASOA) barely changes; isoprene SOA (ISOA) decreases the most as expected since the drought stress factor is  
479 applied to isoprene emissions only. Interestingly, terpene SOA (TSOA) also shows a slight decrease, suggesting  
480 positive feedback between ISOA and TSOA.

481 In summary, the OMI-based drought stress factor shows good performance in correcting the overestimation of  
482 biogenic isoprene in default GEOS-Chem simulations under drought conditions. The drought stress factor was  
483 constrained by the observed exponential fitting between the HCHO to LAI ratio and temperature, not by observed  
484 HCHO columns directly. It nearly eliminates the high HCHO bias compared with OMI observations in the SE US  
485 under drought conditions, which consequently improves the simulation of OA. MDA8 O<sub>3</sub> slightly increases in the  
486 areas with high isoprene emissions, leading to no improvement in model bias but a better agreement with the observed  
487 O<sub>3</sub> increment with drought severity. Places with lower isoprene emissions show an MDA8 O<sub>3</sub> reduction of 1-3 ppbv,  
488 indicating the region-specific O<sub>3</sub> responses to the changes of isoprene due to the nonlinearity of O<sub>3</sub> chemistry.

## 489 **6. Conclusions**

490 Using long-term (JJA 2005-2017) weekly USDM drought index and OMI HCHO column data over the SE US, we  
491 revealed a step-increase pattern of HCHO by 5.3%, 9.7%, 15.3%, 18.7%, and 19.8% from D0 to D4 relative to non-  
492 drought conditions (N0), respectively, which indicates the increasingly higher isoprene emissions with drought on a  
493 regional scale although the rate of increase decreases under severe droughts. Compared with OMI observations, the  
494 GEOS-Chem simulated HCHO column density exhibits a similar pattern, but the changes are 1.4-2.0 times higher  
495 with a respective increase of 10.5%, 15.7%, 21.7%, 25.8%, and 28.9% from D0 to D4. Since there are no big changes  
496 in anthropogenic VOCs under droughts, biogenic isoprene emissions are the key drivers for the increase of HCHO,  
497 and a drought stress factor is missing in the MEGAN2.1 biogenic inventory in the default GEOS-Chem simulations  
498 causing the overestimation of the HCHO changes in response to droughts.



499 The MOFLUX site provides the only long-term ground-based isoprene flux observations covering multiple drought  
500 severities. We developed a drought stress algorithm based on the MOFLUX site following Jiang et al. (2018), and the  
501 algorithm improves the HCHO simulation at the MOFLUX grid while underestimating HCHO after all the SE US  
502 grids are included. By comparison, the OMI-based drought stress algorithm derived from the different HCHO-  
503 temperature sensitivities between OMI and GEOS-Chem can reflect better spatial coverage and nearly removes the  
504 positive bias between OMI and the default simulations seen from a test simulation in May-September 2012 over the  
505 SE US.

506 The long-term simulation with the OMI-based drought stress factor can significantly reduce the biogenic isoprene  
507 emissions by  $0.35 \times 10^{-10} \text{ kg m}^{-2} \text{ s}^{-1}$  (14.24%),  $0.43 \times 10^{-10} \text{ kg m}^{-2} \text{ s}^{-1}$  (16.57%),  $0.49 \times 10^{-10} \text{ kg m}^{-2} \text{ s}^{-1}$  (17.49%),  $0.58 \times 10^{-10}$   
508  $\text{ kg m}^{-2} \text{ s}^{-1}$  (18.66%) and  $0.65 \times 10^{-10} \text{ kg m}^{-2} \text{ s}^{-1}$  (20.74%) from D0 to D4, respectively, which consequently leads to a  
509 better agreement between OMI and simulated HCHO column. Despite lowering emissions relative to the no-stress  
510 simulation, OMI\_Stress\_GC simulates a non-uniform trend of increasing isoprene emissions with drought severity  
511 that is consistent with OMI HCHO and MOFLUX. Relative to N0, the simulated increase in isoprene emissions is 15-  
512 18% under D0-D1, increasing to 26% at D2 and peaking at 37% at D3, followed by a slight decrease to 35% at D4.

513 The observed MDA8 O<sub>3</sub> and OA over the SE US show a similar increase pattern with HCHO. The OMI-based drought  
514 stress algorithm also helps reduce the mean bias of OA by  $0.30 \text{ } \mu\text{g/m}^3$  (6.60%),  $0.46 \text{ } \mu\text{g/m}^3$  (8.98%)  $0.60 \text{ } \mu\text{g/m}^3$   
515 ( $10.07\%$ ),  $0.67 \text{ } \mu\text{g/m}^3$  (10.85%),  $0.62 \text{ } \mu\text{g/m}^3$  (10.88%),  $0.74 \text{ } \mu\text{g/m}^3$  (11.71%) from N0 to D4 over the SE US compared  
516 with the high positive bias of more than  $2.02 \text{ } \mu\text{g/m}^3$  (50.83%) without the drought stress. By contrast, the MDA8 O<sub>3</sub>  
517 response to the reduced biogenic isoprene caused by the drought stress factor presents a spatial disparity due to the  
518 nonlinear O<sub>3</sub> chemistry. Places with high isoprene emissions show an increase of MDA8 O<sub>3</sub> by less than 1 ppbv, which  
519 slightly improves the simulated drought-O<sub>3</sub> relationship. For the regions with low isoprene emissions in the SE US,  
520 the drought stress factor reduces MDA8 O<sub>3</sub> by 1-3 ppbv.

521 This study reveals an increasingly higher level of biogenic isoprene under drought conditions over the regions with  
522 high vegetation coverage. As drought is predicted to become more frequent in a warming climate (Cook et al., 2018),  
523 it is essential to update current biogenic emission inventories by adding a drought stress factor and to improve the  
524 constraints of isoprene chemistry in the climate chemistry models in order to have a better projection of air quality in  
525 the future. We demonstrate the feasibility of applying satellite data to the development of drought stress algorithms  
526 when ground-based measurements are limited. More biogenic emission flux observations covering different  
527 vegetation types and drought severities will be helpful to better depict the relationships between biogenic VOCs and  
528 drought stress.

## 529 **Acknowledgment**

530 This work was supported by NASA Atmospheric Composition Modeling and Analysis Program (80NSSC19K0986).  
531 The development of the ecophysiology module in GEOS-Chem has also been supported by the General Research Fund  
532 (14306220) granted by the Hong Kong Research Grants Council. The authors thank NASA Langley Research Center



533 for the OMI HCHO column data and the National Drought Mitigation Center for making and providing the USDM  
534 maps. Roger Seco was supported by grants RYC2020-029216-I and CEX2018-000794-S funded by  
535 MCIN/AEI/10.13039/501100011033 and by the European Social Fund “ESF Investing in your future”.

#### 536 **Data Availability**

537 GEOS-Chem model is publicly available at <http://www.geos-chem.org>. LAI is obtained from  
538 [http://geoschemdata.wustl.edu/ExtData/HEMCO/Yuan\\_XLAI/v2021-06/](http://geoschemdata.wustl.edu/ExtData/HEMCO/Yuan_XLAI/v2021-06/). O<sub>3</sub> and organic carbon observational data  
539 can be downloaded via [https://aqg.epa.gov/aqgweb/documents/data\\_mart\\_welcome.html](https://aqg.epa.gov/aqgweb/documents/data_mart_welcome.html). Observational isoprene  
540 measurements at MOFLUX are from Potosnak et al. 2014 and Seco et al. 2015 and are available upon request from  
541 co-author Alex Guenther. Satellite ΩHCHO is available publicly at  
542 [https://cmr.earthdata.nasa.gov/search/concepts/C1626121562-GES\\_DISC.html](https://cmr.earthdata.nasa.gov/search/concepts/C1626121562-GES_DISC.html).

#### 543 **Competing interests**

544 The authors declare that they have no conflict of interest.

#### 545 **Author contributions**

546 YW conceived the research idea. NL and WL conducted the model simulation and data analysis. JCYL and APKT  
547 created the ecophysiology module. AG, MJP and RS provided the field observations. All authors contributed to the  
548 interpretation of the results and the preparation of the manuscript

#### 549 **References**

- 550 Abbot, D. S., Palmer, P. I., Martin, R. V., Chance, K. V., Jacob, D. J., and Guenther, A.: Seasonal and interannual  
551 variability of North American isoprene emissions as determined by formaldehyde column measurements from  
552 space, *Geophys. Res. Lett.*, 30, <https://doi.org/10.1029/2003GL017336>, 2003.
- 553 Atkinson, R.: Atmospheric chemistry of VOCs and NO<sub>x</sub>, *Atmos. Environ.*, 34, 2063–2101,  
554 [https://doi.org/10.1016/S1352-2310\(99\)00460-4](https://doi.org/10.1016/S1352-2310(99)00460-4), 2000.
- 555 Best, M. J., Pryor, M., Clark, D. B., Rooney, G. G., Essery, R. L. H., Ménard, C. B., Edwards, J. M., Hendry, M. A.,  
556 Porson, A., Gedney, N., Mercado, L. M., Sitch, S., Blyth, E., Boucher, O., Cox, P. M., Grimmond, C. S. B., and  
557 Harding, R. J.: The Joint UK Land Environment Simulator (JULES), model description – Part 1: Energy and water  
558 fluxes, *Geosci. Model Dev.*, 4, 677–699, <https://doi.org/10.5194/gmd-4-677-2011>, 2011.
- 559 Budisulistiorini, S. H., Baumann, K., Edgerton, E. S., Bairai, S. T., Mueller, S., Shaw, S. L., Knipping, E. M., Gold,  
560 A., and Surratt, J. D.: Seasonal characterization of submicron aerosol chemical composition and organic aerosol  
561 sources in the southeastern United States: Atlanta, Georgia, and Look Rock, Tennessee, *Atmospheric Chem. Phys.*,  
562 16, 5171–5189, <https://doi.org/10.5194/acp-16-5171-2016>, 2016.
- 563 Chance, K.: OMI/Aura Formaldehyde (HCHO) Total Column Daily L3 Weighted Mean Global 0.1 deg Lat/Lon  
564 Grid V003, Goddard Earth Sci. Data Inf. Serv. Cent. GES DISC Greenbelt MD USA, 2019.



- 565 Chang, K.-Y., Xu, L., Starr, G., and Paw U, K. T.: A drought indicator reflecting ecosystem responses to water  
566 availability: The Normalized Ecosystem Drought Index, *Agric. For. Meteorol.*, 250–251, 102–117,  
567 <https://doi.org/10.1016/j.agrformet.2017.12.001>, 2018.
- 568 Chen, L. G., Gottschalck, J., Hartman, A., Miskus, D., Tinker, R., and Artusa, A.: Flash Drought Characteristics  
569 Based on U.S. Drought Monitor, *Atmosphere*, 10, 498, <https://doi.org/10.3390/atmos10090498>, 2019.
- 570 Claeys, M., Graham, B., Vas, G., Wang, W., Vermeylen, R., Pashynska, V., Cafmeyer, J., Guyon, P., Andreae, M.  
571 O., Artaxo, P., and Maenhaut, W.: Formation of Secondary Organic Aerosols Through Photooxidation of Isoprene,  
572 *Science*, 303, 1173–1176, <https://doi.org/10.1126/science.1092805>, 2004.
- 573 Clark, D. B., Mercado, L. M., Sitch, S., Jones, C. D., Gedney, N., Best, M. J., Pryor, M., Rooney, G. G., Essery, R.  
574 L. H., Blyth, E., Boucher, O., Harding, R. J., Huntingford, C., and Cox, P. M.: The Joint UK Land Environment  
575 Simulator (JULES), model description – Part 2: Carbon fluxes and vegetation dynamics, *Geosci. Model Dev.*, 4,  
576 701–722, <https://doi.org/10.5194/gmd-4-701-2011>, 2011.
- 577 Cook, B. I., Mankin, J. S., and Anchukaitis, K. J.: Climate Change and Drought: From Past to Future, *Curr. Clim.*  
578 *Change Rep.*, 4, 164–179, <https://doi.org/10.1007/s40641-018-0093-2>, 2018.
- 579 Fiore, A. M., Horowitz, L. W., Purves, D. W., Levy II, H., Evans, M. J., Wang, Y., Li, Q., and Yantosca, R. M.:  
580 Evaluating the contribution of changes in isoprene emissions to surface ozone trends over the eastern United States,  
581 *J. Geophys. Res. Atmospheres*, 110, <https://doi.org/10.1029/2004JD005485>, 2005.
- 582 Franco, B., Marais, E. A., Bovy, B., Bader, W., Lejeune, B., Roland, G., Servais, C., and Mahieu, E.: Diurnal cycle  
583 and multi-decadal trend of formaldehyde in the remote atmosphere near 46° N, *Atmospheric Chem. Phys.*, 16,  
584 4171–4189, <https://doi.org/10.5194/acp-16-4171-2016>, 2016.
- 585 Geron, C., Daly, R., Harley, P., Rasmussen, R., Seco, R., Guenther, A., Karl, T., and Gu, L.: Large drought-induced  
586 variations in oak leaf volatile organic compound emissions during PINOT NOIR 2012, *Chemosphere*, 146, 8–21,  
587 <https://doi.org/10.1016/j.chemosphere.2015.11.086>, 2016.
- 588 Giglio, L., Randerson, J. T., and van der Werf, G. R.: Analysis of daily, monthly, and annual burned area using the  
589 fourth-generation global fire emissions database (GFED4), *J. Geophys. Res. Biogeosciences*, 118, 317–328,  
590 <https://doi.org/10.1002/jgrg.20042>, 2013.
- 591 Guenther, A., Karl, T., Harley, P., Wiedinmyer, C., Palmer, P. I., and Geron, C.: Estimates of global terrestrial  
592 isoprene emissions using MEGAN (Model of Emissions of Gases and Aerosols from Nature), *Atmospheric Chem.*  
593 *Phys.*, 6, 3181–3210, <https://doi.org/10.5194/acp-6-3181-2006>, 2006.
- 594 Guenther, A. B., Zimmerman, P. R., Harley, P. C., Monson, R. K., and Fall, R.: Isoprene and monoterpene emission  
595 rate variability: Model evaluations and sensitivity analyses, *J. Geophys. Res. Atmospheres*, 98, 12609–12617,  
596 <https://doi.org/10.1029/93JD00527>, 1993.
- 597 Guenther, A. B., Jiang, X., Heald, C. L., Sakulyanontvittaya, T., Duhl, T., Emmons, L. K., and Wang, X.: The  
598 Model of Emissions of Gases and Aerosols from Nature version 2.1 (MEGAN2.1): an extended and updated  
599 framework for modeling biogenic emissions, *Geosci. Model Dev.*, 5, 1471–1492, <https://doi.org/10.5194/gmd-5-1471-2012>, 2012.
- 601 Guenther, A. B., Shah, T., and Huang, L.: A next generation modeling system for estimating Texas biogenic VOC  
602 emissions [M], *AQRP Proj.*, 16–011, 2017.
- 603 Guttman, N. B.: Accepting the Standardized Precipitation Index: A Calculation Algorithm1, *JAWRA J. Am. Water*  
604 *Resour. Assoc.*, 35, 311–322, <https://doi.org/10.1111/j.1752-1688.1999.tb03592.x>, 1999.





- 605 Hoerling, M., Eischeid, J., Kumar, A., Leung, R., Mariotti, A., Mo, K., Schubert, S., and Seager, R.: Causes and  
606 Predictability of the 2012 Great Plains Drought, *Bull. Am. Meteorol. Soc.*, 95, 269–282,  
607 <https://doi.org/10.1175/BAMS-D-13-00055.1>, 2014.
- 608 Huang, J., Dool, H. M. van den, and Georganakos, K. P.: Analysis of Model-Calculated Soil Moisture over the  
609 United States (1931–1993) and Applications to Long-Range Temperature Forecasts, *J. Clim.*, 9, 1350–1362,  
610 [https://doi.org/10.1175/1520-0442\(1996\)009<1350:AOMCSM>2.0.CO;2](https://doi.org/10.1175/1520-0442(1996)009<1350:AOMCSM>2.0.CO;2), 1996.
- 611 Huang, L., McGaughey, G., McDonald-Buller, E., Kimura, Y., and Allen, D. T.: Quantifying regional, seasonal and  
612 interannual contributions of environmental factors on isoprene and monoterpene emissions estimates over eastern  
613 Texas, *Atmos. Environ.*, 106, 120–128, <https://doi.org/10.1016/j.atmosenv.2015.01.072>, 2015.
- 614 Jiang, X., Guenther, A., Potosnak, M., Geron, C., Seco, R., Karl, T., Kim, S., Gu, L., and Pallardy, S.: Isoprene  
615 emission response to drought and the impact on global atmospheric chemistry, *Atmos. Environ.*, 183, 69–83,  
616 <https://doi.org/10.1016/j.atmosenv.2018.01.026>, 2018.
- 617 Kaiser, J., Jacob, D. J., Zhu, L., Travis, K. R., Fisher, J. A., González Abad, G., Zhang, L., Zhang, X., Fried, A.,  
618 Crouse, J. D., St. Clair, J. M., and Wisthaler, A.: High-resolution inversion of OMI formaldehyde columns to  
619 quantify isoprene emission on ecosystem-relevant scales: application to the southeast US, *Atmospheric Chem.*  
620 *Phys.*, 18, 5483–5497, <https://doi.org/10.5194/acp-18-5483-2018>, 2018.
- 621 Kogan, F. N.: Droughts of the Late 1980s in the United States as Derived from NOAA Polar-Orbiting Satellite Data,  
622 *Bull. Am. Meteorol. Soc.*, 76, 655–668, [https://doi.org/10.1175/1520-0477\(1995\)076<0655:DOTLIT>2.0.CO;2](https://doi.org/10.1175/1520-0477(1995)076<0655:DOTLIT>2.0.CO;2),  
623 1995.
- 624 Kravitz, B., Guenther, A. B., Gu, L., Karl, T., Kaser, L., Pallardy, S. G., Peñuelas, J., Potosnak, M. J., and Seco, R.:  
625 A new paradigm of quantifying ecosystem stress through chemical signatures, *Ecosphere*, 7, e01559,  
626 <https://doi.org/10.1002/ecs2.1559>, 2016.
- 627 Lam, J. C. Y. and Tai, A. P.: Development of a New Ecophysiology Module in the GEOS-Chem Chemical  
628 Transport Model to Better Represent Biosphere-Atmosphere Exchange and Ozone-Vegetation Interactions, *Geosci.*  
629 *Model Dev.*, submitted.
- 630 Lei, Y., Yue, X., Liao, H., Zhang, L., Zhou, H., Tian, C., Gong, C., Ma, Y., Cao, Y., Seco, R., Karl, T., and  
631 Potosnak, M.: Global Perspective of Drought Impacts on Ozone Pollution Episodes, *Environ. Sci. Technol.*, 56,  
632 3932–3940, <https://doi.org/10.1021/acs.est.1c07260>, 2022.
- 633 Li, W., Wang, Y., Flynn, J., Griffin, R. J., Guo, F., and Schnell, J. L.: Spatial Variation of Surface O<sub>3</sub> Responses to  
634 Drought Over the Contiguous United States During Summertime: Role of Precursor Emissions and Ozone  
635 Chemistry, *J. Geophys. Res. Atmospheres*, 127, e2021JD035607, <https://doi.org/10.1029/2021JD035607>, 2022.
- 636 Lin, J.-T., Youn, D., Liang, X.-Z., and Wuebbles, D. J.: Global model simulation of summertime U.S. ozone diurnal  
637 cycle and its sensitivity to PBL mixing, spatial resolution, and emissions, *Atmos. Environ.*, 42, 8470–8483,  
638 <https://doi.org/10.1016/j.atmosenv.2008.08.012>, 2008.
- 639 Marais, E. A., Jacob, D. J., Jimenez, J. L., Campuzano-Jost, P., Day, D. A., Hu, W., Krechmer, J., Zhu, L., Kim, P.  
640 S., Miller, C. C., Fisher, J. A., Travis, K., Yu, K., Hanisco, T. F., Wolfe, G. M., Arkinson, H. L., Pye, H. O. T.,  
641 Froyd, K. D., Liao, J., and McNeill, V. F.: Aqueous-phase mechanism for secondary organic aerosol formation from  
642 isoprene: application to the southeast United States and co-benefit of SO<sub>2</sub> emission controls, *Atmospheric Chem.*  
643 *Phys.*, 16, 1603–1618, <https://doi.org/10.5194/acp-16-1603-2016>, 2016.
- 644 McKee, T. B., Doesken, N. J., and Kleist, J.: The relationship of drought frequency and duration to time scales, in:  
645 *Proceedings of the 8th Conference on Applied Climatology*, 179–183, 1993.



- 646 Millet, D. B., Jacob, D. J., Turquety, S., Hudman, R. C., Wu, S., Fried, A., Walega, J., Heikes, B. G., Blake, D. R.,  
647 Singh, H. B., Anderson, B. E., and Clarke, A. D.: Formaldehyde distribution over North America: Implications for  
648 satellite retrievals of formaldehyde columns and isoprene emission, *J. Geophys. Res. Atmospheres*, 111,  
649 <https://doi.org/10.1029/2005JD006853>, 2006.
- 650 Naimark, J. G., Fiore, A. M., Jin, X., Wang, Y., Klovenski, E., and Braneon, C.: Evaluating Drought Responses of  
651 Surface Ozone Precursor Proxies: Variations With Land Cover Type, Precipitation, and Temperature, *Geophys. Res.*  
652 *Let.*, 48, e2020GL091520, <https://doi.org/10.1029/2020GL091520>, 2021.
- 653 Opacka, B., Müller, J.-F., Stavrou, T., Miralles, D. G., Koppa, A., Pagán, B. R., Potosnak, M. J., Seco, R., De  
654 Smedt, I., and Guenther, A. B.: Impact of Drought on Isoprene Fluxes Assessed Using Field Data, Satellite-Based  
655 GLEAM Soil Moisture and HCHO Observations from OMI, *Remote Sens.*, 14, 2021,  
656 <https://doi.org/10.3390/rs14092021>, 2022.
- 657 Pacifico, F., Harrison, S. P., Jones, C. D., and Sitch, S.: Isoprene emissions and climate, *Atmos. Environ.*, 43, 6121–  
658 6135, <https://doi.org/10.1016/j.atmosenv.2009.09.002>, 2009.
- 659 Palmer, P. I., Jacob, D. J., Fiore, A. M., Martin, R. V., Chance, K., and Kurosu, T. P.: Mapping isoprene emissions  
660 over North America using formaldehyde column observations from space, *J. Geophys. Res. Atmospheres*, 108,  
661 <https://doi.org/10.1029/2002JD002153>, 2003.
- 662 Palmer, W. C.: *Meteorological Drought*, U.S. Department of Commerce, Weather Bureau, 68 pp., 1965.
- 663 Potosnak, M. J., LeSturgeon, L., Pallardy, S. G., Hosman, K. P., Gu, L., Karl, T., Geron, C., and Guenther, A. B.:  
664 Observed and modeled ecosystem isoprene fluxes from an oak-dominated temperate forest and the influence of  
665 drought stress, *Atmos. Environ.*, 84, 314–322, <https://doi.org/10.1016/j.atmosenv.2013.11.055>, 2014.
- 666 Pye, H. O. T., Chan, A. W. H., Barkley, M. P., and Seinfeld, J. H.: Global modeling of organic aerosol: the  
667 importance of reactive nitrogen (NO<sub>x</sub> and NO<sub>3</sub>), *Atmospheric Chem. Phys.*, 10, 11261–11276,  
668 <https://doi.org/10.5194/acp-10-11261-2010>, 2010.
- 669 Pye, H. O. T., Murphy, B. N., Xu, L., Ng, N. L., Carlton, A. G., Guo, H., Weber, R., Vasilakos, P., Appel, K. W.,  
670 Budisulistiorini, S. H., Surratt, J. D., Nenes, A., Hu, W., Jimenez, J. L., Isaacman-VanWertz, G., Misztal, P. K., and  
671 Goldstein, A. H.: On the implications of aerosol liquid water and phase separation for organic aerosol mass,  
672 *Atmospheric Chem. Phys.*, 17, 343–369, <https://doi.org/10.5194/acp-17-343-2017>, 2017.
- 673 Schnell, J. L., Holmes, C. D., Jangam, A., and Prather, M. J.: Skill in forecasting extreme ozone pollution episodes  
674 with a global atmospheric chemistry model, *Atmospheric Chem. Phys.*, 14, 7721–7739, <https://doi.org/10.5194/acp-14-7721-2014>, 2014.
- 676 Schroder, J. C., Campuzano-Jost, P., Day, D. A., Shah, V., Larson, K., Sommers, J. M., Sullivan, A. P., Campos, T.,  
677 Reeves, J. M., Hills, A., Hornbrook, R. S., Blake, N. J., Scheuer, E., Guo, H., Fibiger, D. L., McDuffie, E. E., Hayes,  
678 P. L., Weber, R. J., Dibb, J. E., Apel, E. C., Jaeglé, L., Brown, S. S., Thornton, J. A., and Jimenez, J. L.: Sources and  
679 Secondary Production of Organic Aerosols in the Northeastern United States during WINTER, *J. Geophys. Res.*  
680 *Atmospheres*, 123, 7771–7796, <https://doi.org/10.1029/2018JD028475>, 2018.
- 681 Seager, R., Tzanova, A., and Nakamura, J.: Drought in the Southeastern United States: Causes, Variability over the  
682 Last Millennium, and the Potential for Future Hydroclimate Change, *J. Clim.*, 22, 5021–5045,  
683 <https://doi.org/10.1175/2009JCLI2683.1>, 2009.
- 684 Seco, R., Karl, T., Guenther, A., Hosman, K. P., Pallardy, S. G., Gu, L., Geron, C., Harley, P., and Kim, S.:  
685 Ecosystem-scale volatile organic compound fluxes during an extreme drought in a broadleaf temperate forest of the  
686 Missouri Ozarks (central USA), *Glob. Change Biol.*, 21, 3657–3674, <https://doi.org/10.1111/gcb.12980>, 2015.



- 687 Sindelarova, K., Granier, C., Bouarar, I., Guenther, A., Tilmes, S., Stavrou, T., Müller, J.-F., Kuhn, U., Stefani, P.,  
688 and Knorr, W.: Global data set of biogenic VOC emissions calculated by the MEGAN model over the last 30 years,  
689 *Atmospheric Chem. Phys.*, 14, 9317–9341, <https://doi.org/10.5194/acp-14-9317-2014>, 2014.
- 690 Sprengnether, M., Demerjian, K. L., Donahue, N. M., and Anderson, J. G.: Product analysis of the OH oxidation of  
691 isoprene and 1,3-butadiene in the presence of NO, *J. Geophys. Res. Atmospheres*, 107, ACH 8-1-ACH 8-13,  
692 <https://doi.org/10.1029/2001JD000716>, 2002.
- 693 Squire, O. J., Archibald, A. T., Griffiths, P. T., Jenkin, M. E., Smith, D., and Pyle, J. A.: Influence of isoprene  
694 chemical mechanism on modelled changes in tropospheric ozone due to climate and land use over the 21st century,  
695 *Atmospheric Chem. Phys.*, 15, 5123–5143, <https://doi.org/10.5194/acp-15-5123-2015>, 2015.
- 696 Stavrou, T., Müller, J.-F., Bauwens, M., De Smedt, I., Van Roozendaal, M., and Guenther, A.: Impact of Short-  
697 Term Climate Variability on Volatile Organic Compounds Emissions Assessed Using OMI Satellite Formaldehyde  
698 Observations, *Geophys. Res. Lett.*, 45, 8681–8689, <https://doi.org/10.1029/2018GL078676>, 2018.
- 699 Svoboda, M., LeCompte, D., Hayes, M., Heim, R., Gleason, K., Angel, J., Rippey, B., Tinker, R., Palecki, M.,  
700 Stooksbury, D., Miskus, D., and Stephens, S.: THE DROUGHT MONITOR, *Bull. Am. Meteorol. Soc.*, 83, 1181–  
701 1190, <https://doi.org/10.1175/1520-0477-83.8.1181>, 2002.
- 702 Svoboda, M. D., Fuchs, B. A., Poulsen, C. C., and Nothwehr, J. R.: The drought risk atlas: Enhancing decision  
703 support for drought risk management in the United States, *J. Hydrol.*, 526, 274–286,  
704 <https://doi.org/10.1016/j.jhydrol.2015.01.006>, 2015.
- 705 Travis, K. R. and Jacob, D. J.: Systematic bias in evaluating chemical transport models with maximum daily  
706 8&thinsp;h average (MDA8) surface ozone for air quality applications: a case study with GEOS-Chem v9.02,  
707 *Geosci. Model Dev.*, 12, 3641–3648, <https://doi.org/10.5194/gmd-12-3641-2019>, 2019.
- 708 Travis, K. R., Jacob, D. J., Fisher, J. A., Kim, P. S., Marais, E. A., Zhu, L., Yu, K., Miller, C. C., Yantosca, R. M.,  
709 Sulprizio, M. P., Thompson, A. M., Wennberg, P. O., Crouse, J. D., St. Clair, J. M., Cohen, R. C., Laughner, J. L.,  
710 Dibb, J. E., Hall, S. R., Ullmann, K., Wolfe, G. M., Pollack, I. B., Peischl, J., Neuman, J. A., and Zhou, X.: Why do  
711 models overestimate surface ozone in the Southeast United States?, *Atmospheric Chem. Phys.*, 16, 13561–13577,  
712 <https://doi.org/10.5194/acp-16-13561-2016>, 2016.
- 713 Trenberth, K. E., Dai, A., van der Schrier, G., Jones, P. D., Barichivich, J., Briffa, K. R., and Sheffield, J.: Global  
714 warming and changes in drought, *Nat. Clim. Change*, 4, 17–22, <https://doi.org/10.1038/nclimate2067>, 2014.
- 715 Trugman, A. T., Medvigy, D., Mankin, J. S., and Anderegg, W. R. L.: Soil Moisture Stress as a Major Driver of  
716 Carbon Cycle Uncertainty, *Geophys. Res. Lett.*, 45, 6495–6503, <https://doi.org/10.1029/2018GL078131>, 2018.
- 717 Vicente-Serrano, S. M., Beguería, S., and López-Moreno, J. I.: A Multiscalar Drought Index Sensitive to Global  
718 Warming: The Standardized Precipitation Evapotranspiration Index, *J. Clim.*, 23, 1696–1718,  
719 <https://doi.org/10.1175/2009JCLI2909.1>, 2010.
- 720 Wang, Y., Xie, Y., Dong, W., Ming, Y., Wang, J., and Shen, L.: Adverse effects of increasing drought on air quality  
721 via natural processes, *Atmospheric Chem. Phys.*, 17, 12827–12843, <https://doi.org/10.5194/acp-17-12827-2017>,  
722 2017.
- 723 Wells, K. C., Millet, D. B., Payne, V. H., Deventer, M. J., Bates, K. H., de Gouw, J. A., Graus, M., Warneke, C.,  
724 Wisthaler, A., and Fuentes, J. D.: Satellite isoprene retrievals constrain emissions and atmospheric oxidation,  
725 *Nature*, 585, 225–233, <https://doi.org/10.1038/s41586-020-2664-3>, 2020.
- 726 Willeke, G., Hosking, J. R. M., Wallis, J. R., and Guttman, N. B.: The national drought atlas, *Inst. Water Resour.*  
727 *Rep.*, 94, 1994.



- 728 Xu, L., Guo, H., Boyd, C. M., Klein, M., Bougiatioti, A., Cerully, K. M., Hite, J. R., Isaacman-VanWertz, G.,  
729 Kreisberg, N. M., and Knote, C.: Effects of anthropogenic emissions on aerosol formation from isoprene and  
730 monoterpenes in the southeastern United States, *Proc. Natl. Acad. Sci.*, 112, 37–42, 2015.
- 731 Yuan, H., Dai, Y., Xiao, Z., Ji, D., and Shanguan, W.: Reprocessing the MODIS Leaf Area Index products for land  
732 surface and climate modelling, *Remote Sens. Environ.*, 115, 1171–1187, <https://doi.org/10.1016/j.rse.2011.01.001>,  
733 2011.
- 734 Zheng, Y., Unger, N., Tadić, J. M., Seco, R., Guenther, A. B., Barkley, M. P., Potosnak, M. J., Murray, L. T.,  
735 Michalak, A. M., Qiu, X., Kim, S., Karl, T., Gu, L., and Pallardy, S. G.: Drought impacts on photosynthesis,  
736 isoprene emission and atmospheric formaldehyde in a mid-latitude forest, *Atmos. Environ.*, 167, 190–201,  
737 <https://doi.org/10.1016/j.atmosenv.2017.08.017>, 2017.
- 738 Zheng, Y., Thornton, J. A., Ng, N. L., Cao, H., Henze, D. K., McDuffie, E. E., Hu, W., Jimenez, J. L., Marais, E. A.,  
739 Edgerton, E., and Mao, J.: Long-term observational constraints of organic aerosol dependence on inorganic species  
740 in the southeast US, *Atmospheric Chem. Phys.*, 20, 13091–13107, <https://doi.org/10.5194/acp-20-13091-2020>,  
741 2020.
- 742 Zhu, L., Jacob, D. J., Kim, P. S., Fisher, J. A., Yu, K., Travis, K. R., Mickley, L. J., Yantosca, R. M., Sulprizio, M.  
743 P., De Smedt, I., González Abad, G., Chance, K., Li, C., Ferrare, R., Fried, A., Hair, J. W., Hanisco, T. F., Richter,  
744 D., Jo Scarino, A., Walega, J., Weibring, P., and Wolfe, G. M.: Observing atmospheric formaldehyde (HCHO) from  
745 space: validation and intercomparison of six retrievals from four satellites (OMI, GOME2A, GOME2B, OMPS)  
746 with SEAC<sup>4</sup>RS aircraft observations over the southeast US, *Atmospheric Chem. Phys.*, 16, 13477–13490,  
747 <https://doi.org/10.5194/acp-16-13477-2016>, 2016.

748